Quantifiying the effect of amyotrophic lateral sclerosis on the neural and non-neural properties of the wrist

D.J.L. Stikvoort García

TU Delft

Quantifying the effect of amyotrophic lateral sclerosis on the neural and non-neural properties of the wrist

MASTER OF SCIENCE THESIS

For the degree of Master of Science in Mechanical Engineering at Delft University of Technology

D.J.L. Stikvoort Garcìa

December 16, 2019

Faculty of Mechanical, Maritime and Materials Engineering (3ME) at Delft University of Technology

This thesis project was carried out at, and supported by the UMC Utrecht and the ALS foundation of the Netherlands.

DELFT UNIVERSITY OF TECHNOLOGY
MECHANICAL ENGINEERING

TRACK: BIOMECHANICAL DESIGN
SPECIALIZATION: HAPTIC INTERFACES

The undersigned hereby certify that they have read and recommend to the faculty of Mechanical, Maritime and Materials Engineering (3ME) for acceptance of the thesis entitled:

QUANTIFYING THE EFFECT OF AMYOTROPHIC LATERAL SCLEROSIS ON THE NEURAL AND NON-NEURAL PROPERTIES OF THE WRIST

By:

D.J.L. Stikvoort Garcìa

In partial fulfilment of the requirements for the degree of:

MASTER OF SCIENCE IN MECHANICAL ENGINEERING

To be defended publicly on monday December 16th , 2019 at 10:00 AM.

Chair of the examination committee:

Prof. dr. ir. F.C.T. van der Helm

Supervisors:

Dr. ir. J.M. Meier (UMC Utrecht)

Dr. ir. B.T.H.M. Sleutjes (UMC Utrecht)

Readers:

Dr. ir. W. Mugge

Dr. ir. M. Wiertlewski


TU Delft

D.J.L. Stikvoort Garcìa
Delft, December 16th 2019

PREFACE

Before you lies the master thesis "Quantifying the effect of amyotrophic lateral sclerosis on the neural and non-neural properties of the wrist", which describes the first attempt to bring system identification and parameter techniques to the field of motor neuron diseases. It has been written to fulfil the graduation requirements for becoming a Master of Science in mechanical engineering at Delft University of Technology. From November 2018 till February 2019 I was engaged in writing a literature study as part of the initial work of the thesis. Since February I have been engaged in writing the main thesis.

The majority of the work was carried out at and supported by the University Medical Centre of Utrecht (UMCU). My research goal was formulated in collaboration with the chair of the examination committee, prof. dr. ir. F.C.T. van der Helm. As a student from an engineering background, suddenly being immersed in the medical world was a difficult, yet rewarding experience. Writing a full proposal for the medical ethics committee of the UMCU was particularly one of the most difficult parts of this thesis project. However, finally being granted the right to perform the study of 5 months of hard work, was amazing. It gave me the chance to work with an incredibly motivated patient group, despite their vulnerable state. Recruiting participants myself, talking to them on the phone and sensing their enthusiasm to help in the field of ALS research, was very inspiring. Performing the study hard at some times, but it allowed me to demonstrate the potential of an unexplored technique to kickstart novel ALS research.

I would like to sincerely thank my supervisors, Jil Meier and Boudewijn Sleutjes, for their incredible support throughout this 13 month process. The level of dedication they put into their guidance of me has helped me to build up a study of which I could not have dreamed when starting out. Furthermore I would like to express my gratitude to prof. dr. ir. F.C.T. van der Helm, for accepting to be the chair of the defense committee and my head supervisor. His enormous experience in this field was incredibly inspiring and useful. In addition, I would like to thank dr. ir. W. Mugge and dr. ir.M. Wiertlewski for accepting to be in my defense committee.

To my colleagues in the lab of the UMCU: I would like to thank you for always being available to answer questions about the clinical aspects of ALS and several other pathologies, as well as your support in patient interaction.

Lastly, I'm extremely grateful to my family, my girlfriend and my friends for endlessly supporting me for better or worse. Your faith in what I was doing and your loving counsel has helped me get to where I am now.

Contents

ABSTRACT

Amyotrophic lateral sclerosis (ALS) is the most frequent form of motor neuron diseases (MND). This neurodegenerative disease progresses relentlessly quick. The characteristic feature of ALS is the concurrent degeneration of the upper and lower motoneurons (UMN & LMN) in the central and peripheral nervous system. Symptomatic behavior in ALS is the result of complex symptom interplay, as well as symptom counteraction. Therefore, adequate examination of motor function in ALS requires an examination technique that quantifies disease symptoms at their origin, rather than at their point of expression. The goal of this study was to quantify and explore the effect of ALS on intrinsic and reflexive properties of the limbs of the patients under passive and active conditions. To the best of our knowledge, this study was the first to assess a MND within this particular framework.

A group of 10 ALS patients and 9 controls were recruited for participation in an extensive protocol, comprising of several motor tasks and maximal voluntary contraction measurements. The tasks were performed on a single-axis wrist manipulator, which produced multisine torque perturbations. A linear system identification and parameter estimation procedure was implemented to estimate the parameters of a neuromuscular model with 5 task-dependent (2 intrinsic, 3 reflexive) and 8 task-independent parameters.

All participants were able to fully comply with the study protocol and indicated that the effort required for the tasks was easily maintained. Variance of the intrinsic parameters was generally increased in the patient group, with a tendency towards a reduced median. The median of the reflexive parameter muscle spindle position dependence was significantly increased in ALS patients during a relax task. Additionally, reflexive and intrinsic parameters of individual patients were frequently found to be responsive to the patients respective clinical state. Muscle stiffness during the relax task was strongly correlated to the summed average EMG in ALS patients ($r = 0.75$, $p = 0.013$). During active tasks, three main control strategies were derived from the intrinsic and reflexive parameters in patients.

We show that our study protocol is viable for examination of ALS patients within a large range of physical capacity. The use of quantitative parameters allowed us to disentangle fundamentally overlapping UMN and LMN symptoms. The derived parameters were shown to enhance clinical scores within their respective clinical definitions. Lastly, our results offer new insights beyond the current clinical knowledge of motor function under active conditions in ALS.

Quantifying the effect of amyotrophic lateral sclerosis on the neural and non-neural properties of the wrist

D.J.L. Stikvoort García

I. INTRODUCTION

Amyotrophic lateral sclerosis (ALS) is the most frequent form of motor neuron diseases (MND) [1], a group of neurodegenerative diseases. Within the first weeks to months after disease onset, the upper and lower motoneurons (UMN & LMN) in the central and peripheral nervous system start to degenerate [2]. This process induces a variety of symptoms. Typical signs of UMN degeneration are hyperreflexia, weakness, spasticity and rigidity [3]. Degeneration of the LMN causes hyporeflexia, paresis, paralysis, atrophy and hypotonia [4, 5]. The expression of these symptoms is highly influenced by differences in progression rate and the clinical heterogeneity of the disease. In the absence of definite tests, clinical examination of ALS is based on the interpretation of symptoms [1]. Clinicians frequently resort to the use of ordinal scales to grade the severity of symptoms. Unfortunately, these clinimetrics are not an accurate enough reflection of the origin of factors that contribute to the observed pathological behavior [6, 7]. The main cause behind this notion is the complex interplay and counteracting effects of UMN and LMN symptoms.

Human motor behavior, either healthy or pathological, can be considered in terms of contributions from an intrinsic and reflexive pathway, Figure 1A. The intrinsic pathway describes the voluntary contributions to motor behavior, i.e. the facilitation from supraspinal activity. An example of voluntary motor behavior is holding up an empty cup of coffee and waiting for it to be filled, 1B. However, the muscles also need to compensate for the increasing weight of the cup as it is filled. This process occurs involuntarily through the incorporation of sensory information via the reflexive pathway. Humans continuously adapt the properties of the components on these pathways to improve task performance in daily life activities [8]. Within this framework, symptoms of ALS can be considered faulty properties of these pathways' components, Figure 1C. On the reflexive pathway, hyperreflexia is induced by a decrease in presynaptic inhibition [9]. Spasticity is the result of muscle hypertonia with a velocity-dependent resistance to muscle stretching [10], which is also expressed over the reflexive pathway. Muscle weakness as a result of UMN loss is expressed on the intrinsic pathway. These symptoms are exclusively expressed under voluntary contraction, integration of sensory information or increased baseline muscle activity. Therefore, these particular traits of the UMN syndrome are considered of neural origin. Most of the LMN symptoms are also of neural origin, as degeneration of the α- and γ-motoneurons results in suppression of both intrinsic and reflexive muscle activity [11, 12]. However, UMN and LMN dysfunction are also accompanied by symptoms that are consequential to muscular properties and not muscle activity, i.e. non-neural. An example of such a symptom is rigidity, which originates from secondary changes in the biomechanical properties of muscles, tendons and connective tissues [6, 13-19]. In syndromes with LMN degeneration, such as ALS, the loss of LMN results in atrophy and hypotonia [4]. These symptoms of non-neural origin form an additional branch in the intrinsic pathway. A schematic representation of the expression of symptomatic behavior as a result of symptom interaction is depicted in Figure 1C.

Adequate examination of motor function in ALS requires a procedure that quantifies the disease symptoms at their origin, rather than at their point of expression. For this purpose, symptoms should be re-characterized as a set of altered neural and muscular properties, whose interaction produces motor behavior. One of the main challenges of this framework is posed by the closed-loop behavior of the reflexive pathway [20-22]. This challenge is illustrated in the example of the filling cup, at the stage where reflexive contributions are compensating for the additional weight of the liquid. The generated muscle activity then results from combined intrinsic and reflexive contributions, which again produce new reflexive behavior. This coupling between total muscle activity and reflexive contributions coexists in a so-called closed-loop system. Therefore, examination of motor function requires the implementation of closed-loop system identification (SI) techniques [8]. The SI procedure relies on the application of very accurate perturbations to the limbs, with the use of robotic manipulators [8, 20, 23-26]. During the perturbations, measurements of the elicited motion, force and muscle activity are obtained. The amplitude (gain) and time delay (phase) of the relation between measures and perturbations can be depicted in a frequency response function (FRF). Subsequently, these FRFs can be fitted onto a neuromuscular model (NMM). A NMM is a mathematical description of the interaction between the nervous system and the muscles. Within a robotics

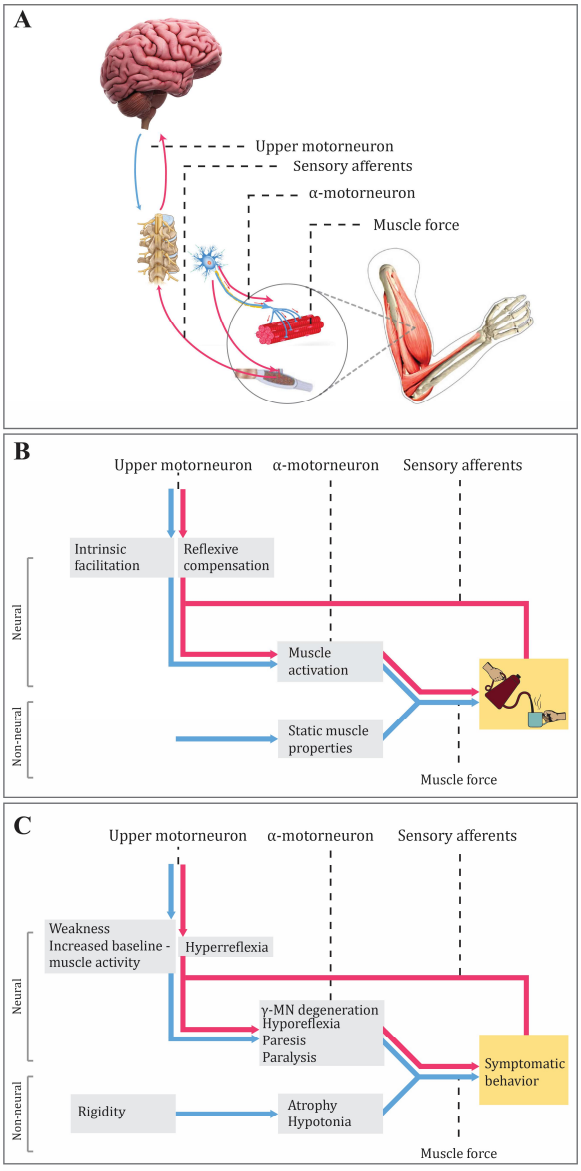

Figure 1 A) The physiological presentation of the neuromuscular system, governing human motor behavior. The intrinsic pathway and reflexive pathway are presented in blue and pink, respectively. B) Schematic presentation of the neuromuscular system when holding a filling a cup. The neural components (gray boxes) are adapted for optimal task performance. C) Schematic presentation of the neuromuscular system in ALS patients. Symptoms (gray boxes) are depicted as faulty properties of the components on the intrinsic and reflexive pathways.

paradigm, the nervous system acts as the controller of the body, whereas the muscles act as actuators. The interaction between these systems to produce motor behavior is described by the model in a similar manner as depicted in Figure 1. As a result, the NMM can be used to translate the limb dynamics into physiologically representative parameters [24, 27-29]. At the moment, the implementation of SI techniques and parameter estimation on NMM in ALS research remains yet unexplored. However, several studies in the field of UMN diseases have shown these techniques' potential for application in clinical practice. In stroke and cerebral palsy, intrinsic and reflexive parameters were found to be responsive to clinical scores of rigidity and spasticity [30-33]. Furthermore, reflex modulation was found to be impaired in stroke patients when performing active tasks [18]. In Parkinson's disease, reflexive and intrinsic parameters had a non-significant tendency to increase in patients with poorer motor scores [34, 35]. From a diagnostics perspective, many of these studies were able to find significant differences between the patient and control groups [30-35]. These studies were able to advance the understanding of the origins of pathological motor behavior in their respective fields. Therefore, this technique could be applied in ALS to disentangle the concurrent effects of UMN and LMN symptoms, by assessing them in terms of intrinsic and reflexive parameters. The non-invasive and inexpensive nature of measurements required in a model-based approach, make them well suited for implementation alongside current clinical practices. Such an approach could move the state of motor function examination from interpretation of symptoms towards an assessment with quantitative biomarkers.

The goal of this study was to quantify and explore the effect of ALS on the intrinsic and reflexive properties of the limbs of patients. This study is the first to implement SI and parameter estimation techniques in ALS. Therefore, a large portion of this study was dedicated to the examination of the validity of the approach. From a clinical perspective, this study aimed to estimate neuromechanical parameters for the enhancement of clinical scores of disease progression. Ultimately, these parameters could serve as a set quantitative measures that recognize the heterogeneous nature of ALS. To explore multiple facets of symptomatic behavior, intrinsic and reflexive properties need to be triggered under different conditions. Therefore, an extensive experimental protocol was implemented to explore ALS patients under active and passive conditions.

II. METHODS

A. *Participants*

A group of 10 patients diagnosed with definite, probable or possible ALS according to the revised El Escorial criteria [36] was recruited from the outpatient clinic of the University Medical Centre Utrecht, The Netherlands. The group characteristics are presented in Table 1. Patients on medication known to have an association with motorneuron dysfunction were excluded from the study. Further exclusion criteria were the presence of active psychiatric diseases, medical conditions associated with neuropathies, history or presence of brain injury, epilepsy or other cerebral diseases. For the control group, 9 healthy participants were recruited, Table 1. The Medical Ethics Committee of Utrecht approved this study. All participants provided their written informed consent prior to the experiment.

Table 1 The characteristics of the study population. The muscle strength, muscle tone and reflexes are all taken from the right arm.

	Characteristic	Controls	ALS
Participants	N (male)	9 (6)	10 (7)
	Age (median, IQR)	61 (60.00 – 62.75)	59 (54.25 – 67.00)
	Months since diagnosis (median, IQR)	n.a.	13.6 (9.31 – 17.1)
ALSFRS-R score	Total (median, IQR) , max = 48	n.a.	38 (32 – 40)
	Arm (median, IQR), max = 8	n.a.	6 (6 – 8)
Muscle strength arm	Summed MRC (median, IQR), max = 35	n.a.	34 (30 – 35)
Muscle tone arm	Hypo, norm, hyper	n.a.	0, 9, 1
Reflexes arm	Absent, low, normal, elevated, hyper	n.a.	0, 1, 1, 6, 2

B. *Experiment setup*

At the start of the experiment, participants were seated in a chair with their elbows slightly flexed and their feet supported, approximately 2 m in front of a screen. The screen provided the participants with task instructions and visual feedback to avoid drift from the target force or position during the tasks. The skin of the right forearm was cleaned and abraded and two sets of bipolar surface electrodes were placed on the flexor and extensor carpi radialis muscles (FCR and ECR, respectively) [37, 38]. The electrodes were placed in the centre of the muscle belly on the line from origin to insertion, as determined by muscle palpation. Muscle activation was measured with a TMSi REFA amplifier (TMSi, Oldenzaal, The Netherlands). A Wristalyzer single-axis wrist manipulator [39] (MOOG FCS, Nieuw Vennep, The Netherlands) was set up to apply unpredictable multisine torque perturbations with a duration of 35s to the wrist, which elicited small angle excursions (SD ≈ 1°). The perturbation level required to achieve this range of angle excursions was examined in each task. For this purpose, the perturbation level was defined by the root-mean-square of the perturbation signal. The design of the perturbation signal design is discussed in depth in Appendix A. The range of motion of the Wristalyzer was limited to fit the participant's own range of motion, which was measured prior to the experiment. The rotation axis of the wrist was aligned with the rotation axis of the Wristalyzer. Isolated movement of the wrist was ensured by fixating the hand and forearm with Velcro straps to the handle and the foam-padded forearm support respectively, Figure 2.

C. *Signal preprocessing*

The EMG, wrist torque and angle measurements were recorded and stored at a sample frequency of 2048 Hz. To ensure accurate estimation of muscle activity from the EMG data, measurements were processed as described in detail elsewhere [28, 40]. Briefly, EMG recordings were bandpass filtered bidirectionally (20-450 Hz, 3rd order Butterworth) to remove artefacts, DC components and noise. A prewhitening filter was applied to reduce the variance of the EMG amplitude estimate [40]. The filtered EMG was rectified and normalized with respect to the average of the maximum EMG values during maximum voluntary contraction (MVC). This process allows for inter-subject comparison at a later stage [41]. Lastly, all the recorded and processed signals were resampled at 128 Hz to reduce computational load during the parameter estimation procedure.

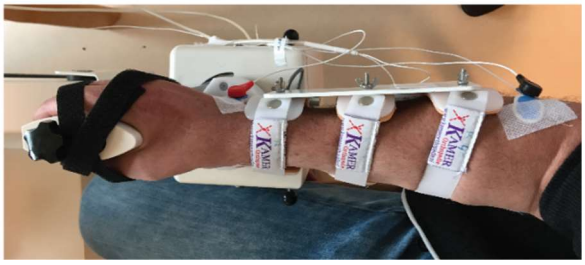

Figure 2 The experimental setup of the experiment. Participants were attached with Velcro to the forearm support and handle of a single axis wrist manipulator (Wristalyzer, MOOG FCS, Nieuw Vennep, the Netherlands), which applied multisine torque perturbations to the wrist. The resulting wrist torque and angle were measured, as well as the muscle activation of the FCR and ECR muscle.

D. *Experimental protocol*

Prior to the experiment, participants received a short briefing on what to expect during the experimental protocol. For this study, a protocol was adapted from Mugge et al. [41] and expanded with additional tasks. First, three MVC measurements with a duration of 6s were performed in flexion and extension. Depending on the level of strength of the participant, the MVC measurement was performed either with a handheld dynamometer or the Wristalyzer. The dynamometer was necessary as the Wristalyzer cannot withstand high levels of torque. After these preliminary recordings, three types of tasks were performed under continuous application of torque perturbations:

- Relax task (RT): minimize muscle activity to ensure passive behavior.
- Force task (FT): maintain a constant force level by complying with the perturbations.
- Position task (PT): maintain a fixed position by resisting the perturbations.

Whereas the RT and PT were performed only once, the FT was performed twice, at a force level of 10% and 20% of the MVC torque ($FT_{10\%}$ and $FT_{20\%}$). Prior to the recording of the task, a short practice session was performed. In this session the task was explained in

depth and trained. The phases between the mechanical and EMG signals were observed by the researcher as an indication of task performance. Hereafter, the tasks were performed in ascending order of expected physical effort, i.e. RT-FT$_{10\%}$-FT$_{20\%}$-PT. A total of three trials were recorded per task, generating a set of 12 measurements per individual. Participants received up to 1 minute of rest between trials, although longer resting periods were allowed if requested. After each task, participants received 3 minutes of rest during which the next task was explained. The total duration of the experiment was approximately 45 minutes.

E. *System identification and parameter estimation*

To derive a set of physiologically interpretable neuromuscular parameters for each participant, a parameter estimation procedure was implemented. For this purpose, the integral dynamical properties of the limbs were described in two FRFs [24, 28, 42-47]. The FRF of limb displacements to muscle force characterizes the susceptibility of the joint to movement: the joint admittance [24]. The joint admittance is best interpreted as a level of compliance to disturbances. A higher admittance indicates that a joint is more easily displaced with less force. The FRF of muscle activity from EMG to limb displacement characterizes the reflexive activity during muscle stretching: the reflexive impedance [47]. The first step of the procedure was to derive the joint admittance and reflexive impedance of each trial and task. Hereafter, the model parameters were derived by fitting a neuromuscular model onto the FRFs. During the last step of the procedure, the internal and external validity of the modelled system were examined. These three steps are described further in the next subsections. An overview of all the steps in the parameter estimation procedure is supplied in Appendix B.

1) Joint admittance and reflexive impedance

A closed-loop SI procedure was used to estimate the FRFs of the participants wrist. The FRFs were derived as follows,

$$\hat{H}_{T\theta}(f) = \frac{\hat{S}_{d\theta}(f)}{\hat{S}_{dT}(f)} \quad (1)$$

$$\hat{H}_{\theta a}(f) = \frac{\hat{S}_{da}(f)}{\hat{S}_{d\theta}(f)} \quad (2)$$

$\hat{H}_{T\theta}(f)$ denotes the joint admittance and $\hat{H}_{\theta a}(f)$ the reflexive impedance, respectively. The functions $\hat{S}_{dA}(f)$, $\hat{S}_{d\theta}(f)$ and $\hat{S}_{dT}(f)$ denote the cross-spectral densities between the perturbation signal and the combined EMG from the flexor and extensor e_{flexor} and $e_{extensor}$, the wrist angle θ_{wrist} and the wrist torque T_c, respectively. In addition, f is a vector containing all the frequencies up to the highest excited frequency by the perturbation signal. Note that by convention, frequency-domain signals are denoted by a capital letter, in contrast to their time-domain counterparts. Welch's method was applied to improve the quality of the estimates [48]. FRFs are typically depicted in terms of their magnitude $|\hat{H}_{T\theta}(f)|$ and phase $\angle\hat{H}_{T\theta}(f)$. Figures

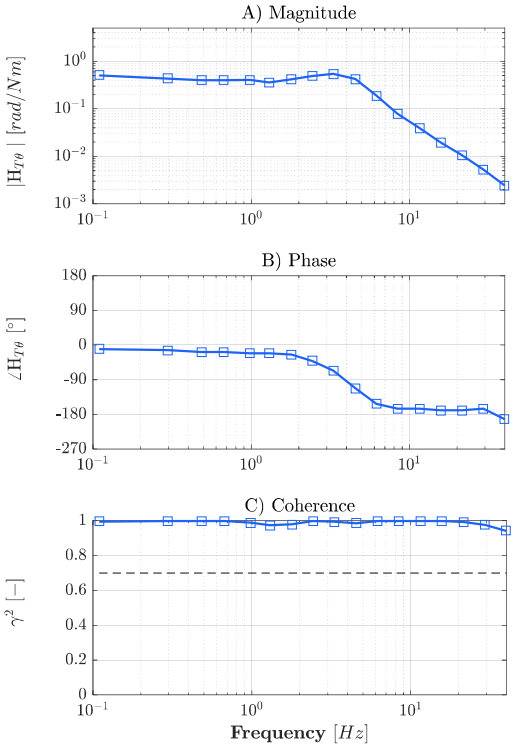

Figure 3 A-B) Example of a typical FRF of the wrist joint admittance during an RT. A) Depicts the magnitude $|\hat{\boldsymbol{H}}_{T\theta}(\boldsymbol{f})|$ in rad/Nm. B) Depicts the phase $\angle\hat{\boldsymbol{H}}_{T\theta}(\boldsymbol{f})$ in degrees. C) depicts the coherence $\boldsymbol{\gamma_{d\theta}}^2(\boldsymbol{f})$ of the system, in which the dashed line indicates a coherence of 0.7 (i.e. linear assumption fulfilled). The markers indicate the frequencies at which the wrist was stimulated, ranging from 0.1-40 Hz.

3A-3B depict a typical example of an FRF of the estimated joint admittance during an RT. An important aspect of this non-parametric SI technique is that the spectral density is estimated under the assumption of linearity. A frequently applied measure to evaluate the quality of spectral density estimators is the coherence [49], defined by:

$$\gamma_{d\theta}{}^2(f) = \frac{|\hat{S}_{d\theta}(f)|^2}{|\hat{S}_{dd}(f)\hat{S}_{\theta\theta}(f)|} \quad (3)$$

$$\gamma_{dA}{}^2(f) = \frac{|\hat{S}_{dA}(f)|^2}{|\hat{S}_{dd}(f)\hat{S}_{AA}(f)|} \quad (4)$$

Where $\hat{S}_{dd}(f)$, $\hat{S}_{\theta\theta}(f)$ and $\hat{S}_{AA}(f)$ denote the respective auto-spectral densities of the perturbation signal, the wrist angle θ_{wrist} and the combined EMG from the flexor and extensor e_{flexor} and $e_{extensor}$, respectively. The coherence produces values between 0 and 1, where lower values indicate the increasing dominance of non-linearities and low signal-to-noise ratios (SNR) in the spectral estimators. A coherence above 0.7 was considered good, i.e. the spectral estimator fulfills the imposed assumption of linearity [50]. Figure 3C depicts the corresponding coherence to the estimated FRF.

2) Parameter estimation procedure

This study implemented the NMM from the Matlab package NMCLab [45]. The full derivation of the

Table 2 All the parameters derived during parameter estimation. This table presents the initial condition for the estimation procedure, as well as the lower and upper bounds (LB and UB, respectively). These bounds ensure that the parameter values remain within a physiologically plausible range. *Task-dependent parameters were estimated in all four tasks (RT, $FT_{10\%}$, $FT_{20\%}$, PT) and three trials (4x3).

Type	Name	Physiological representation	Initial value	LB	UB	Unit
Task-independent	I	Wrist inertia	0.05	0.001	0.05	Kgm^2
	b_c	Contact dynamics, viscosity	150	100	250	Nms/rad
	k_c	Contact dynamics, stiffness	250	100	1000	Nm/rad
	k_{tend}	Tendon stiffness	1000	500	10000	Nm/rad
	τ_{ms}	Neural delay, muscle spindles	0.04	0.015	0.08	ms
	τ_{gto}	Neural delay, Golgi tendon organ	0.03	0.015	0.07	ms
	f_a	Muscle activation dynamics, eigenfrequency	5	3.5	10	Hz
	β	Muscle activation dynamics, relative damping	0.75	0.5	1.5	-
Task-dependent	b	Intrinsic muscle viscosity	1	0.05	5	Nms/rad
(4 x 3)*	k	Intrinsic muscle stiffness	5	1	30	Nm/rad
	k_p	Muscle spindle position dependence	2	-20	20	Nm/rad
	k_v	Muscle spindle velocity dependence	0	-5	5	Nms/rad
	k_f	Golgi tendon organ force dependence	0.01	-2	2	Nm/rad

model is explained in Appendix C. The output of the model is determined by 13 parameters in total (see Table 2). The intrinsic pathway's contribution to the limb dynamics is described by 2 task-dependent parameters. These parameters are muscle stiffness k and muscle viscosity b. It is assumed that b and k are related to the amount of muscle contraction. On the reflexive pathway of the NMM, 3 parameters characterize the contribution of the proprioceptive organs to the limb- and neural dynamics. The first parameter is force dependent resistance kf, originating from excitation of the type Ib afferents from the Golgi tendon organs. The second and third parameters denote the muscle spindle's responses to muscle stretch and muscle stretch rate, kp and kv respectively. These parameters relate to the excitation levels of the type II and type Ia afferents from the muscle spindles. The remaining 8 parameters are considered to be constant for each individual participant, irrespective of task. These parameters characterize wrist inertia I, contact dynamics (stiffness k_c, viscosity b_c), tendon stiffness k_{tend} and muscle activation dynamics (eigenfrequency f_a, relative damping β). To account for neural delays of the sensory system, the influence of reflexive parameters on motor behavior is delayed. These delays in the system influence the phase of the FRF. Therefore, the NMM exploits the characteristic properties of the human body to quantify intrinsic and reflexive parameters. All NMM parameters were simultaneously estimated for each participant by minimizing a logarithmic error function in a least-squares sense [46].

$$E = \sum_f \sum_i \frac{\gamma_{d\theta}{}^2(f)}{1+f} \left| log\left(\frac{\hat{H}_{T\theta,i}(f)}{H_{T\theta,i}(f,p)}\right)\right|^2 + \frac{q_i \gamma_{dA}{}^2(f)}{1+f} \left| log\left(\frac{\angle\hat{H}_{\theta A,i}(f)}{\angle H_{\theta A,i}(f,p)}\right)\right|^2 + pm^2 \quad (5)$$

The $\hat{H}$ indicates the FRF estimate of the measurements and H the output of the NMM, respectively. In addition, i denotes the task condition and f is a vector containing the excited frequencies by the perturbation signal. The left-hand term contains the full joint admittance. The middle term only contains the phase of reflexive impedance, as its gain is ambiguous [47]. The entire right hand term was scaled by the coefficient q_i to approximately 10% of the end value of the left hand term. This entry augmented the reliance on the mechanical signals over EMG signals. In addition, more emphasis was placed on frequencies with a higher coherence. The third term was introduced as a stability criterion, where pm denotes the phase margins of the total system. For this term, only negative values were used, which suggest that the total system is unstable. Lastly, the parameter vector to optimize is denoted by p, consisting of 68 parameters (5x4x3 task-dependent and 8 task-independent), Table 2. An important consideration is that overparameterization of the neuromuscular system makes parameter estimation susceptible to local minima. To consistently obtain the best solution over all participants, the initial values of the parameter vector are optimized as well. This optimization is achieved by examining multiple initial conditions. The initial condition yielding the lowest error value is chosen as the definitive starting point. In addition, parameter bounds were set to avoid physiologically implausible results. The general initial conditions and parameter limits for all the participants are also listed in Table 2.

3) Internal validity

The internal validity of the model fit was examined via assessment of the covariance matrix P [30, 51]

$$P = \frac{1}{N}(J^T J)^{-1} \cdot E \cdot E^T \quad (6)$$

With E is the final prediction error, N the number of samples in E and J the Jacobian containing the gradients of the error function, respectively. The cross-covariances of matrix P describe the interdependence between the parameters. The values of the covariance matrix were normalized by the auto-correlations on the diagonal of the matrix. Hence, interdependence was expressed in percentages, with 0% being no interdependence and 100% being full dependence. The auto-correlations provide an indication of the sensitivity of the parameters. The sensitivity was expressed in standard error of the mean (SEM), which was calculated by taking the square root of the auto-correlations of P. Similar to parameter interdependence, the SEM was assessed in percentages with respect to the parameter it represents. A lower SEM indicates that a small change in parameter value leads to a large deviation of the error function. Hence, parameters with a lower SEM can be considered more sensitive.

4) External validity

The external validity of the model fit was assessed with the variance accounted for (VAF). The VAF indicates if a model is able to accurately approximate the real behavior.

$$VAF_i = \left[1 - \frac{\sum_n^N (y_{1,i}(t) - y_{2,i}(t))^2}{\sum_n^N y_{1,i}(t)^2}\right] \cdot 100\% \qquad (7)$$

The signals $y_{1,i}(t)$ and $y_{2,i}(t)$ denote the measurement data and model-predicted data of task i, respectively. The VAF is examined between sample number n and N. In this study, the first and last 3 seconds of samples from the signals were omitted in the VAF calculation, to reduce transient effects from filters and integrators in the NMM [41].

F. *Statistics*

Median differences between the task-dependent parameters of the patient and control groups were assessed with Wilcoxon rank-sum tests. The differences in variance of the task-dependent parameters were examined with Levene's test. The relation between intrinsic muscle properties and quantified effort was assessed with Pearson's correlation coefficient.

III. RESULTS

A. *Measurements*

The participants were all able to comply with the study protocol. All recordings of the tasks (19x12 = 228 in total) were used for the estimation of the NMM parameters. An example of the measurements in time-domain from a typical patient is supplied in Appendix D. Participants indicated that the effort required for the tasks was easily maintained. Physical effort was quantified as the summed average of the normalized and rectified flexor and extensor EMG. The tasks of the study protocol consistently required more effort from the ALS patients than controls, Figure 4A. In one case, a participant with ALS requested longer periods of rest during and between the $FT_{20\%}$ and the PT due to fatigue. This patient had high levels of effort in all tasks, but particularly during the RT. The effort required from this patient is depicted in Figure 4A with pink crosses.

During the preliminary recordings, 8 out of 10 MVC measurements in the ALS group were performed with the handheld dynamometer. The maximum voluntary contraction (MVC) measurements in the control group were all performed with the handheld dynamometer. The variance in the ALS group was larger than in the

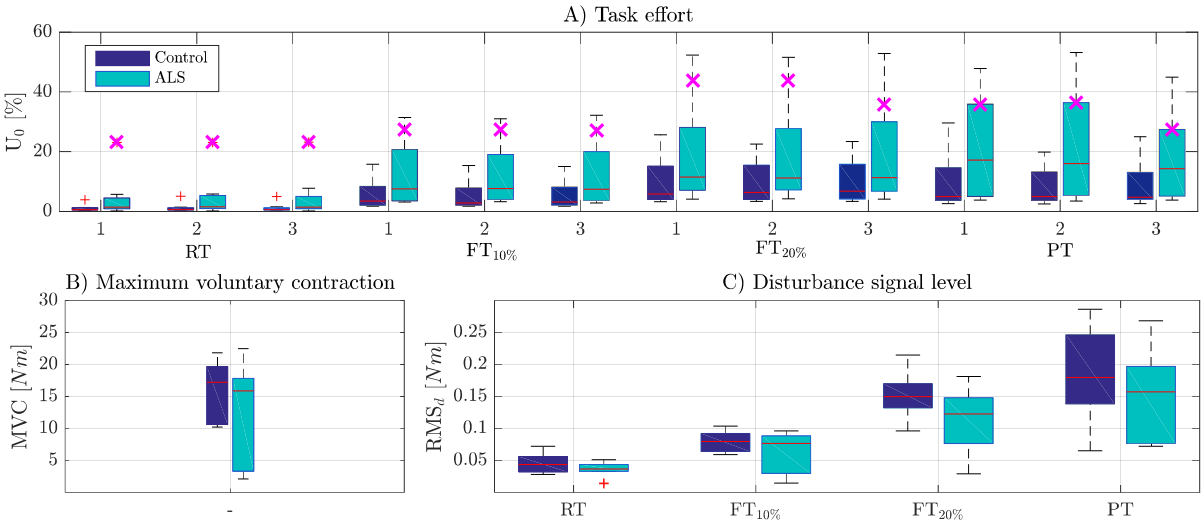

Figure 4 Boxplots of several derived measures from the study protocol depicting the median (red lines), 25th and 75th percentiles (box edges), 95% confidence intervals (whiskers) and outliers (red crosses). The plots depict A) An overview of the measured task effort U_0 for each trial (1-3) and task of both the control and ALS group, B) the MVC measurements in flexion direction, C) the perturbation signal level RMS_d for each group for all the tasks.

controls, indicative of the heterogeneous presentation of the disease, Figure 4B.

The ALS patients were on average subjected to a lower perturbation signal level RMS_d than the controls, Figure 4C. The value of this level was the result of limiting the wrist angle motion to SD ≈ 1°. Larger variances were found in the perturbation signal level RMS_d of the ALS group during FTs. Contrastingly, the variance in the perturbation signal level RMS_d of the RT was smaller in the ALS group than in the control group.

B. *Experimental and modeled FRFs*

The closed-loop SI procedure yielded FRFs of joint admittance and reflexive impedance for each task and trial. The FRFs were most consistently estimated during the RT and PT. The consistency during the FTs was slightly lower but acceptable. All derived joint admittances from one patient are presented in Appendix D, as well as one model fit. On average, the ALS patients had a slightly higher joint admittance during the RT than controls. During the FTs and PTs, group averages were not visually distinguishable. Though, large individual differences were identified in the admittances of the patient group.

1) Relax task admittance comparison

The admittance magnitudes of 4 weaker patients (ALS07-ALS10), a patient without noticeable weakness in the arm (ALS02) and a control (C05) are presented in Figure 5A. The magnitude at low frequencies is indicative of muscle stiffness. However, the resting admittance of the limbs of ALS patients was not fully dependent on muscle strength alone, as suggested by the grouping in Figure 5B.

2) Position task admittance comparison

The admittances derived from the PT of the same participants are presented in Figure 5C. Several characteristic properties of the FRF of weaker patients were different compared to the presented control and stronger patient. In this task participants were expected to decrease their admittance by modulating their reflexive and intrinsic properties. The control (C05) and unaffected patient (ALS02) were able to decrease their admittance much further than the weaker patients . Furthermore, the total range of the magnitude from these two participants was much larger than that of the weaker patients. A remarkable characteristic of the FRF of weaker patients was a down-shift in the frequency of the resonance peak, Figure 5D. The resonance peak was determined at the frequency where the phase drops below -90°. A strong correlation between muscle strength and resonance frequency was found in the patient group ($r = 0.79$, $p = 0.0062$). By comparison, no correlation was found in the control group ($r = -0.041$, $p = 0.91$).

3) Force task admittance comparison

The admittance from the FTs of the control (C05) and two weaker patients (ALS07, ALS09) are presented in Figure 5E-F. Only three cases are presented in these figures to avoid illegibility. The magnitude at the lowest frequency was expected to relate to the bias torque level that had to be maintained. The difference in admittance of both patients during $FT_{10\%}$ suggests that ALS07 was subjected to a lower bias torque than ALS09. However, the bias torque levels imposed on these patients were comparable, which indicates that ALS07 was better able to comply with the perturbations than ALS09. During $FT_{20\%}$, both patients performed comparably. In the higher frequency regions of FRF, a shift in resonance frequency similar as during the PT was identified in all participants. However, in most cases the resonance frequency was lower than during the PT.

4) Quality of the spectral estimates

In several cases, the FRFs contained a second resonance peak at frequencies between 1-1.5Hz. In the control group, this artefact occurred 6 times in all PT FRFs and 4 times in all $FT_{20\%}$ FRFs. In the ALS group, the same artefact was found 4 times in all PT and $FT_{20\%}$ FRFs. The coherence was generally acceptable across all participants ($\gamma^2 > 0.7$), although some large dips were observed between 1-5Hz. An example of these coherence dips from a typical patient is supplied in Appendix D. These dips were predominantly found in the FTs and PT, yet were not bound to a specific group. As a result, both groups had comparable coherences throughout all tasks. The average coherence of the control and ALS group for each task is depicted in Table 3A.

C. *Parameter estimation results*

1) Internal model validity

Examination of the covariance matrix from the parameter estimation procedure yielded 9x68 = 612 and 10x68 = 680 SEMs for the control and ALS patient group respectively. In both groups, more than 99% of the SEM values were below 10%. Consequently, the low SEM values indicate that the model parameters were sensitively determined [30]. A figure presenting the average SEMs per parameter and task, as well as their standard deviations, is shown in Appendix E. Interdependence of the parameters was also low in almost all cases. Out of a total of 68x68x9 = 41616 interdependences in the control group, only 7 were found above 10%. In the ALS group, only 1 interdependence value above 10% was found out of the 68x68x10 = 46240. Consequently, the parameters from both groups can be considered independently estimated. The average interdependence between the parameters of the groups is also presented in Appendix E.

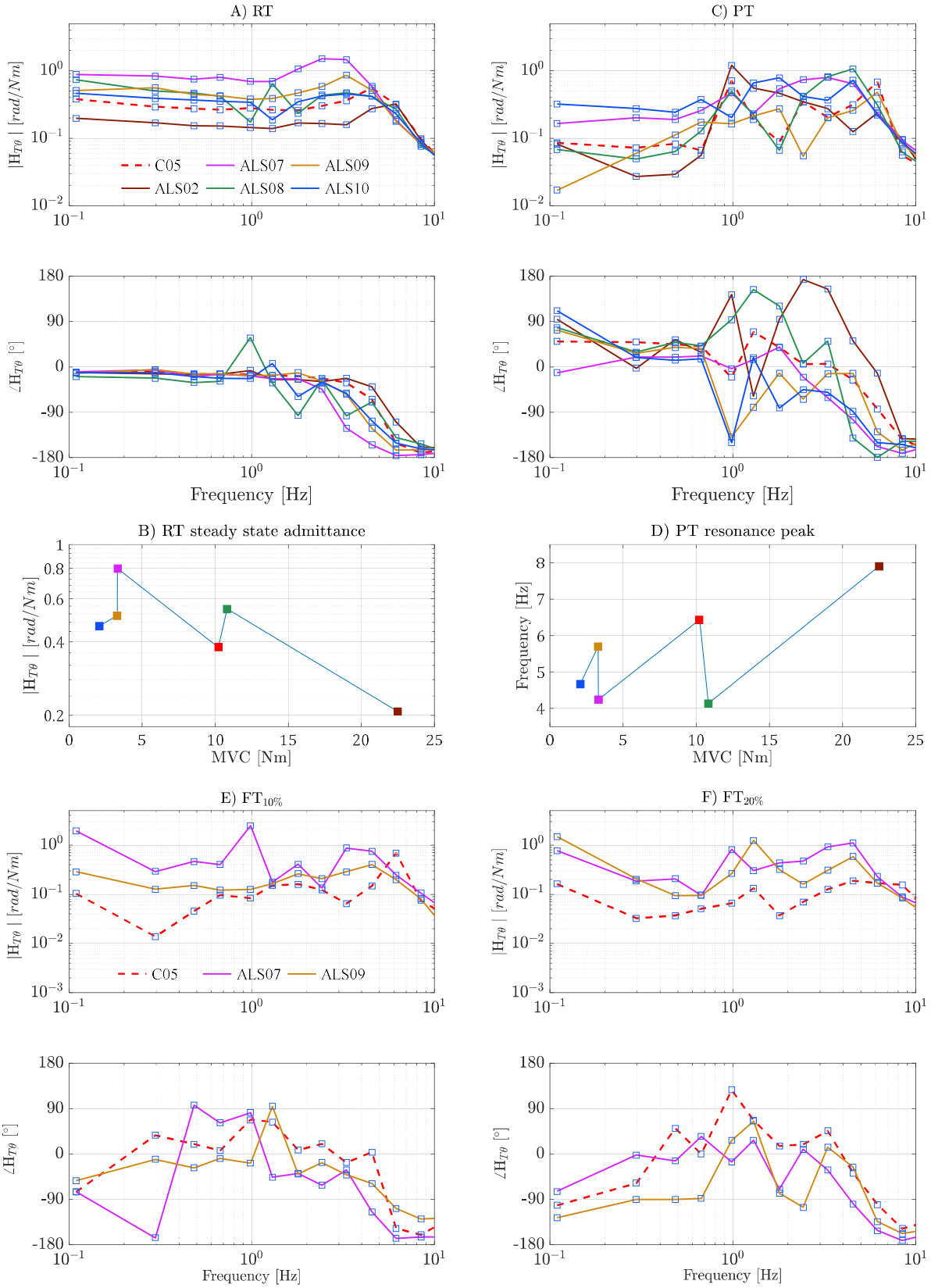

Figure 5 A) The FRFs (magnitude $\left|\widehat{\boldsymbol{H}}_{\boldsymbol{T\theta}}\right|$ and phase $\angle\widehat{\boldsymbol{H}}_{\boldsymbol{T\theta}}$) from the RT of 1 control (C05, red dashed) and 5 ALS patients (ALS02, ALS07-ALS10 in brown, pink, green, yellow and blue, respectively). B) The x-axis represents the participants respective MVC measurements. The y-axis depicts the admittance magnitude of the same participants as in A) at the lowest excited frequency. C) The FRFs from the PT of the same participants as in A). D) The x-axis represents the participants respective MVC measurements. The y-axis depicts the participants' corresponding resonance frequency during the PT. E) The FRFs from the $FT_{10\%}$ of 1 control (C05, red dashed line) and 2 ALS patients (ALS07, ALS09 in pink and orange solid lines, respectively) . F) The FRFs from the $FT_{20\%}$ of the same participants as in E).

Table 3 A) The mean task coherences of the wrist angle ($\gamma_{d\theta}^2$) and muscle activity (γ_{dA}^2) and their respective standard deviations. B) The mean variance accounted for (VAF) and standard deviations of the simulated wrist torque T_c and wrist angle θ_{wrist} in percentages from the control and ALS groups.

A	Wrist angle coherence, $\gamma_{d\theta}^2$ (SD) (%)				EMG coherence, γ_{dA}^2 (SD) (%)			
	RT	$FT_{10\%}$	$FT_{20\%}$	PT	RT	$FT_{10\%}$	$FT_{20\%}$	PT
Controls	92.2 (16.1)	81.3 (24.1)	84.5 (22.6)	78.7 (25.2)	51.9 (28.6)	55.6 (28.9)	56.3 (29.4)	56.9 (30.2)
Patients	92.3 (15.1)	78.3 (25.2)	79.8 (25.7)	79.5 (25.4)	50.3 (28.7)	54.6 (29.6)	55.4 (28.9)	54.8 (30.3)

B	Wrist torque VAF, T_c (SD) (%)				Wrist angle VAF, θ_{wrist} (SD) (%)			
	RT	$FT_{10\%}$	$FT_{20\%}$	PT	RT	$FT_{10\%}$	$FT_{20\%}$	PT
Controls	91.2 (2.47)	82.8 (8.09)	77.8 (9.59)	95.5 (0.78)	83.8 (8.60)	46.5 (12.4)	38.5 (17.5)	33.2*(24.6)
Patients	84.6 (13.3)	78.3 (10.8)	74.1 (12.6)	95.6 (0.89)	83.2 (7.59)	43.4 (14.0)	39.6 (10.9)	41.7 (18.3)

*Two outlying sub-zero VAFs in the PT were set to zero to avoid large distortion of the mean and SD.

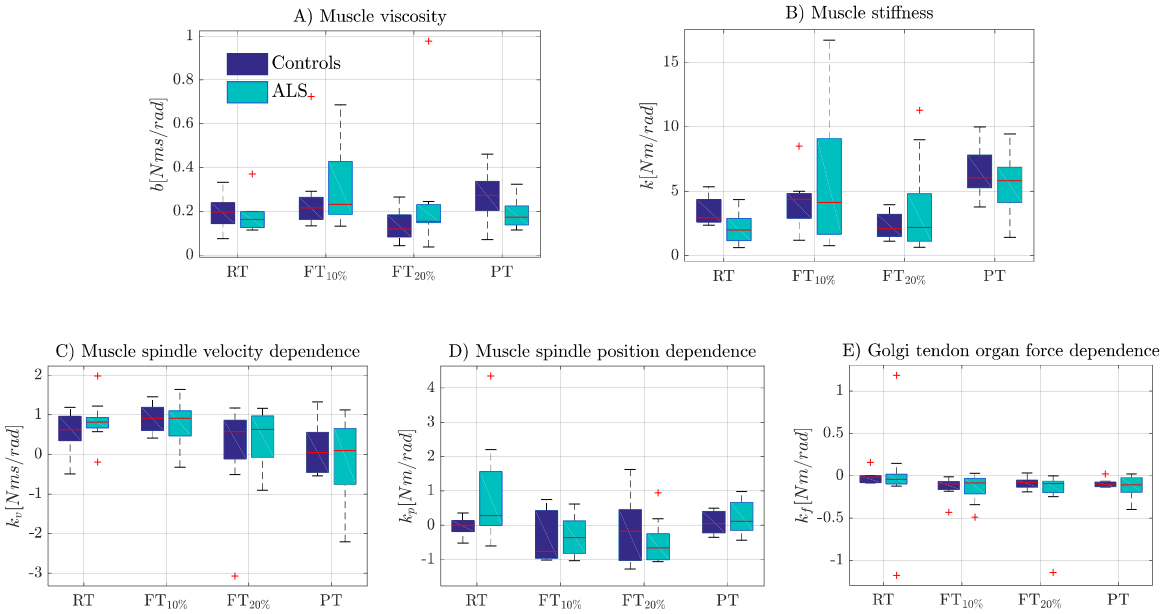

Figure 6 Boxplots of the task-dependent parameters from the NMM depicting median (red lines), 25th and 75th percentiles (box edges), 95% confidence intervals (whiskers) and outliers (red crosses) for controls (dark blue) and patients (light blue).The plots depict A) muscle viscosity *b*, B) muscle stiffness *k*, C) muscle spindle velocity dependence k_v, D) muscle spindle position dependence, k_p, and E) Golgi tendon organ force dependence, k_f.

2) External model validity

In most cases, if the simulation of the NMM yielded comparable VAFs between the trials, then parameter sets were also comparable. Therefore, further analysis of the data was based on parameter sets from the trial that produced the highest VAFs per task. A table containing the best individual VAFs of all participants is supplied in Appendix E. Generally, the VAFs corresponding to the simulated wrist torque T_c were good. The best values were found during the PT, Table 3B. The lowest values were obtained while simulating the FTs. The biggest difference in the VAF of wrist torque T_c between the controls and ALS patients was found during the RT. The simulated wrist angle θ_{wrist} yielded lower but comparable VAFs in both groups. Acceptable values were found when simulating the RT. However, VAF values from the simulation of the FTs and PT were lower. In three controls (C02, C03, C04), only negative VAFs were found for the simulated wrist angle θ_{wrist} of the PT. Therefore, the corresponding parameters sets of the PT have been omitted from further analysis.

3) Neuromuscular parameters

The median intrinsic muscle parameters (*b*, *k*) of the ALS patients were frequently lower than in the controls, Figure 6A-B. In this figure, the intrinsic parameters from the FTs have been corrected by the corresponding bias torques. As such, these parameters can be compared between participants. Intrinsic parameter differences were particularly visible in the low tail of the boxplots. The observed tendencies of the medians and variances follow the distribution of the MVC values, as depicted in Figure 4B. Although, no significant differences were found between the ALS group and the control group. In rest, muscle

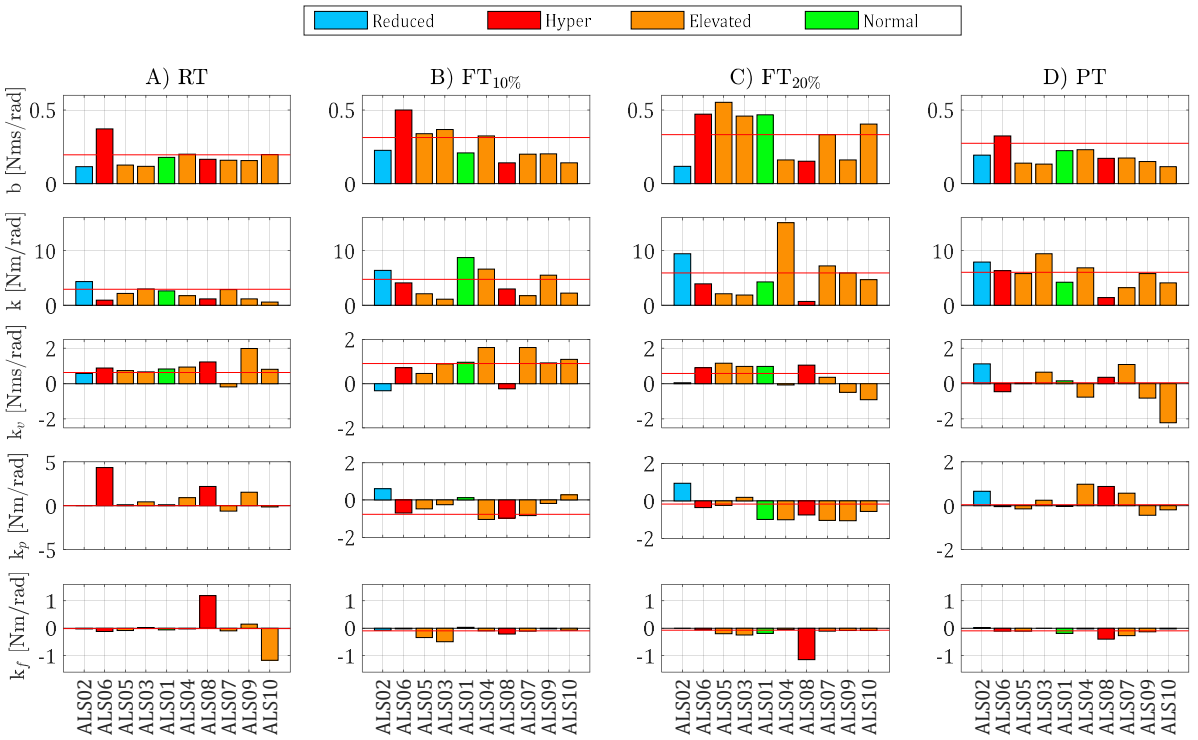

Figure 7 Bars depict the intrinsic and scaled reflexive parameters of each single patient (denoted on the x-axis), sorted by the strength level from left to right, i.e. ALS02 the strongest. The bar-color represents the reflex scores from Table 1: reduced (blue), normal (green), elevated (orange) and hyper (red). The median parameter value from the control group is given as reference (red line). The columns depict A) the RT, B) the $FT_{10\%}$, C) the $FT_{20\%}$ and D) the PT.

stiffness k of the patients during the RT was strongly correlated with the quantified effort ($r = 0.75$, $p = 0.013$). This relation was neither strong nor significant in the control group ($r = 0.33$, $p = 0.36$).

The reflexive parameters were scaled with the intrinsic parameters. As such, the combined effect of these parameters on motor behavior can be better interpreted. Note that the reflexive parameters are discussed in terms of inhibitory or excitatory function. Conventionally, positive dependence on muscle spindle feedback is considered excitatory, whereas positive dependence on Golgi tendon organ feedback is considered inhibitory. At rest, the median scaled muscle spindle position dependence k_p was much more excitatory in ALS patients than in controls ($p = 0.012$), Figure 6C-E. In addition, the variance of the scaled muscle spindle velocity dependence k_v was reduced in patients, concurrent with a more excitatory median value. Differences between reflexive parameters were less obvious in tasks that required active behavior. Only the variance of the Golgi tendon organ force dependence had a tendency to be increased in patients.

The individual patient parameters from each task are presented in Figure 7. The corresponding values are presented in Table 5 of Appendix F. The patients were ordered from left to right in order of descending MVC. In addition, the reflexive score was given by the color of the bars. At rest, some patients (ALS06, ALS08, ALS09) had a considerably more excitatory muscle spindle position dependence k_p with respect to muscle stiffness k than controls. Patients ALS06 and ALS08 both had hyperreflexia, ALS09 had signs of elevated reflexes. In two other patients (ALS03, ALS04), the same value was found to slightly more excitatory. Again, this finding was consistent with the elevated reflexes of both patients. Patient ALS10 was an interesting case with elevated reflexes. This patient' muscle spindle position dependence k_p was slightly more inhibitory, alongside a considerably large excitatory Golgi tendon organ force dependence k_f.

When examining the active tasks, three types of control strategies were found during the $FT_{10\%}$, Figure 8. These strategies mainly revolve around the adaptation of the intrinsic muscle stiffness k. The "normal" strategy was defined by regulation of muscle stiffness to approximately the required level (ALS01, ALS02, ALS04). However, no clear tendencies were found in the reflexive parameters of patients using this strategy. The "down" strategy was defined by down-regulation of muscle stiffness below the stiffness required to maintain the bias torque (ALS03, ALS05, ALS06, ALS07). Though, much larger reflexive parameters were identified in these cases. The "up" strategy was defined by over-regulation of muscle stiffness (ALS08, ALS09, ALS10). This strategy was mainly applied by weak patients with elevated or hyperactive reflexes. When switching towards a higher

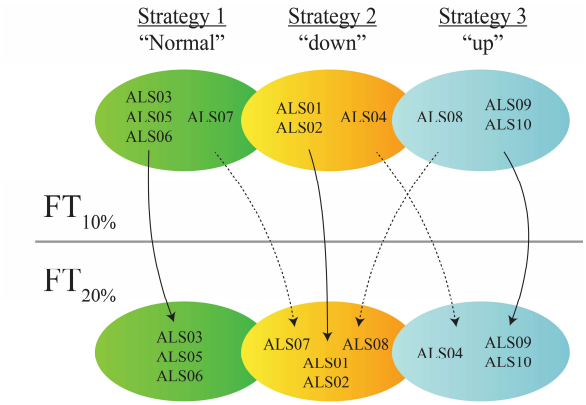

Figure 8 Schematic representation of the grouping of patients into specific control strategies during the FTs. The upper grouping relates to the $FT_{10\%}$, the lower grouping relates to the $FT_{20\%}$. The solid arrows indicate patient(s) that maintained a similar strategy, whereas the dashed arrows indicate a strategy change.

bias level during $FT_{20\%}$, similar control strategies were maintained between participants with comparable clinical features. In contrast to the RT, patients with recognized hyperreflexia and elevated reflexes (ALS06, ALS08 and ALS03, ALS05, ALS04) were able to inhibit their muscle spindle position dependence when performing active tasks. At the most demanding level, i.e. the PT, weaker patients visibly relied much more on modulation of reflexive parameters than reflexive parameters.

IV. DISCUSSION

This study showed the feasibility of performing an extensive protocol on ALS patients to disentangle the effects of UMN and LMN symptoms. A significant part of this study focused on the validity of the parameter estimation procedure. From a clinical perspective, the aim was to derive neuromuscular properties that enhance neurological examination scores and recognize the heterogeneity of the disease.

A. *Study protocol*

The study protocol consisting of relax (RT), force (FT) and position tasks (PT) successfully elicited a range of different control strategies in the participants. The RT and PT were typically performed well even without training. However, the performance on the FTs required some training, but improved quickly. Nevertheless, the more intuitive nature of the RTs and the PT generated more consistent measurements, see Appendix D. Adaptation of the intensity of the perturbation signal and bias torque levels made it possible to use linear SI techniques in a patient group with large strength differences.

B. *Experimental and modeled FRFs*

The average group admittance of ALS patients during the RT was found to be visibly lower than in the control group. In the other tasks, differences were difficult to find based on visual inspection alone. Generally, in low and high frequency ranges (from 0.1-1 Hz and 6-40Hz), derived joint admittances were consistent with findings from other studies [24, 28, 41, 43, 47].

1) Quality of the spectral estimates

In the middle range of frequencies, the frequency response functions (FRFs) of some participants showed multiple resonance peaks in the active tasks. An example of a control with such peaks during the PT is presented in Figure 9A. The likely origin of these peaks is physiological, such as a slow loop of the force or position feedback. However, due to imposed bounds on the neural delays, the implemented NMM was not able to produce two resonance peaks. As a result, a mismatch between the modeled and estimated FRFs was found. In addition to the parameter bounds, the model fit was guided by an error function with more emphasis on low frequencies. Consequently, the modeled resonance peak was shifted more towards the low-frequency resonance peak of the FRF estimate. A short modeling study is presented in Appendix G, in which the most likely origin of the additional peak was investigated. The main contributing factor was concluded to be visual feedback. A model with additional visual feedback provided a better approximation of the FRF estimated than the original model, Figure 9B. The corresponding delay of the visual feedback loop was $\tau_{visual} = 250$ms. The modeled FRF now contained two distinguishable resonance peaks. The newly derived patterns in the task-dependent parameters were consistent with the patterns from the original NMM. Although, their exact values were slightly altered. As such, the originally derived parameters are considered viable for studying (modulation) patterns. From a purely quantitative perspective, a model with visual feedback presents a more accurate representation of human dynamics.

Large dips were present in the coherences of several ALS patients and controls in the range of 1-6Hz, in comparison to similar studies [44, 46], see Appendix D. A reduced coherence indicates either non-linearities, noise or both. The coherences were derived directly from the measurements of a trial, without averaging. Therefore, some noise was undoubtedly captured by the coherence. Another possible cause, is time-variant behavior throughout measurements. This behavior mainly relates to switches in control strategy. Time-variant behavior introduces non-linearities into the spectral estimate [52]. For example, a participant receives a visual cue that prompts him/her to rely more on visual feedback for the performance of tasks. This rationale is further supported by the 1-6Hz range in which the dips occurred. The range starts at the limit of visual feedback limit and ends at the muscle activation dynamics eigenfrequency.

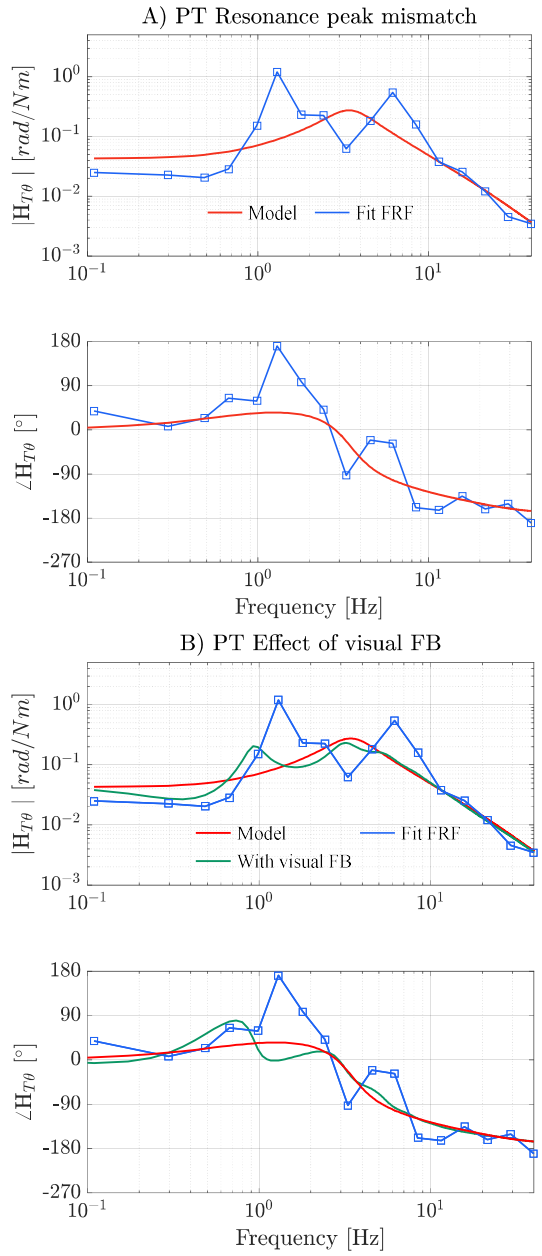

Figure 9 A) The FRF (magnitude $|\widehat{\boldsymbol{H}}_{\boldsymbol{T\theta}}|$ and phase $\angle\widehat{\boldsymbol{H}}_{\boldsymbol{T\theta}}$) from the joint admittance of a control during the PT with multiple resonance peaks. The model fit (red) was performed on the FRF of trial 2 (blue). B) Comparison of the FRFs from the original model from A) (red), and a model with visual feedback (green), fitted on the same FRF (blue).

C. *Parameter estimation*

1) Internal validity

The SEMs of the estimated parameters were typically low in both the control and patient groups. As such, the parameters can be considered accurately estimated. An earlier study noted that neural delay estimates benefit from a larger contribution of the reflexive impedance to the error function [47]. Therefore, SEM values could be further decreased by manipulating the chosen value for q_i, the weighting of the reflexive impedance in the error function, Eq. 5. A short analysis was performed on 5 randomly selected participants (controls and ALS patients) to examine the effect of q_i on the validity of the model fit. The value of q_i was increased to produce an equal final error of the left and middle term of the error function. As a result, the SEMs of the neural delays were reduced by a factor 4. However, the larger contribution of the reflexive impedance decreased the variance accounted for (VAF, Eq. 7) of the simulated wrist angle by approximately 5-10%. A tradeoff between the internal and external validity appears to be present in the parameter estimation procedure. The choice of q_i is not trivial and may depend on several factors. For example, a higher signal to noise ratio can be achieved when the average task EMG is used instead of the EMG from separate trials. In such a scenario, a completely different q_i can be required.

2) External validity

High levels of VAF were found for the wrist angle θ_{wrist} and wrist torque T_c during the RT. Slightly lower levels were found in the VAFs of wrist torque T_c during the FTs. Still, the average VAF in the FTs was higher than in a study with comparable task descriptions (VAF T_c = 74.1% vs. VAF T_c = 39.0%) [41]. The VAFs of the wrist angle during the other tasks were low, ranging on average from 33.2% in the PT to 46.5% in $FT_{10\%}$. In comparison, the aforementioned study had an average VAF of 78.8% during the PT and 85.1% during the FT. A decrease in VAF can be caused by measurement noise, originating from inconsistent performance of the participants. This study did not average over the trials, but rather used all trials for deriving parameter sets. By examining every trial directly, abnormalities in the measurements related to pathological behavior are less likely to be averaged out. However, averaging significantly increases the signal to noise ratio, which reduces the VAF of the wrist torque and wrist angle simulated by the model. In addition to noise, a decrease in VAF can also be an indicator that the model does not fully capture the behavior of the wrist. Expanding the model with visual feedback as described earlier, did not lead to an increase in VAF. Consequently, the most likely factor causing the low VAF of wrist angle θ_{wrist} is noise.

3) Neuromuscular parameters

The general inhibition and excitation patterns of both groups' reflexive parameters from the RT and PT related well to previous findings. In the RT, reflexive parameters were spread around zero; in the PT inhibitory muscle spindle velocity dependence k_v and position dependence k_p were found, opposed by excitatory Golgi tendon organ force dependence k_f [24, 41, 43]. An earlier study implemented an FT without bias forces and found inhibitory muscle spindle position dependence k_p and Golgi tendon organ force dependence k_f [41]. However, the introduction of two levels of bias torque led to excitatory Golgi tendon

organ force dependence k_f. Most likely, this difference originated from the use of a spring to elicit the bias torques during the FTs. The spring produces a resonance peak, which shifts to lower frequencies if the stiffness is reduced. Thus, the identified shifting of the resonance frequency during the FTs was most likely induced by the Wristalyzer, Figures 5E-F. The presence of a sharp resonance peak in the Wristalyzer's own admittance reduces the stability margins of the total system. The excitatory Golgi tendon organ force dependence k_f appeared to act as a stabilizing mechanism. This stabilizing effect of Golgi tendon organ feedback has already been identified during the performance of a PT [41].

D. *Clinical implications*

1) Examination at rest

Several weaker patients could be differentiated from stronger patients and controls, based on visual inspection of the FRFs. During the RT, the admittance at low frequencies was not only dependent on muscle strength. For example, strength differences between patients ALS08 and ALS10 were large, though their resting admittance was comparable, see Figure 5A-B. In cases with negligible resonance peaks, such a phenomenon suggests increased muscle tone of the weaker patient. In cases with a more pronounced resonance peak, excitatory reflexive activity is more likely to be the cause. Such alterations relate well to the classical presentation of UMN degeneration, i.e. hypertonia, spasticity and hyperreflexia [53]. Despite the presence of LMN symptoms, classical UMN symptoms were still captured by the FRFs. The NMM fitted on the FRFs produced sets of neuromuscular parameters that related well to clinical scores. For example, overexcitation position and velocity afferents from the muscle spindles (type II-Ia, respectively) was found in both hyperreflexive patients (ALS06 and ALS08). Hyperreflexia in ALS is most commonly associated with hyperexcitability of the type Ia afferents of the muscle spindle [54]. However, these findings suggest that more (complex) reflexive pathways might be involved. A particularly interesting case further supported this hypothesis. Patient ALS10 was the weakest of the ALS group and the only one with recognized hypertonia. Remarkably, muscle stiffness k did not appear to be significantly increased to the extent that it would be experienced as hypertonia. However, the patient's force afferents from the Golgi tendon organs (type Ib) were extremely overexcited. This mechanism reduces the joint admittance. Therefore, the experienced increase in muscle tone could have originated from hyperreflexia of the type Ib afferents of the Golgi tendon organs instead. Eliciting activity of the type II-Ib afferents requires either a maneuver that relies on complex polysynaptic pathways or larger joint deviations [55]. In clinical examination, muscle tone is often determined by displacing the joint over its range of motion and "feeling" the resistance [56]. In this study, the use of a set of neuromuscular parameters allowed us to simultaneously assess multiple reflexive and intrinsic pathways. The derived parameters indicate that both monosynaptic reflexes (type Ia) and polysynaptic reflexes (type II-Ib) affect symptomatic behavior in ALS. Hence, the effect of polysynaptic stretch reflexes can be obscured by, or even confused with muscle stiffness. This finding is further supported by the notion that interneuron wiring is disrupted by the degenerative process of the disease, as was emphasized by Sherrington school of physiology [57]. In electrophysiological studies, muscle tone is often determined in relation to baseline muscle activity from EMG [56]. The findings of this study indicate a strong correlation between the quantified muscle stiffness k and effort U_0 at rest. As a result, the use of a NMM can functionally enhance clinical and electrophysiological examination with physiologically interpretable parameters.

2) Examination of active task performance

When performing the FTs, three control strategies were derived from the patients' individual parameters, see Figure 8. The "down" strategy involved a reduction in muscle stiffness k, with a large reliance on reflexive activity. The "up" strategy involved an increased muscle stiffness with reduced reflexive activity during $FT_{10\%}$ and increased reflexive activity during $FT_{20\%}$. A possible mechanism behind the choice of strategy, originates from the interaction of the motor cortex with the spinal cord: via direct and indirect projections [58, 59]. The motor cortex projects to the

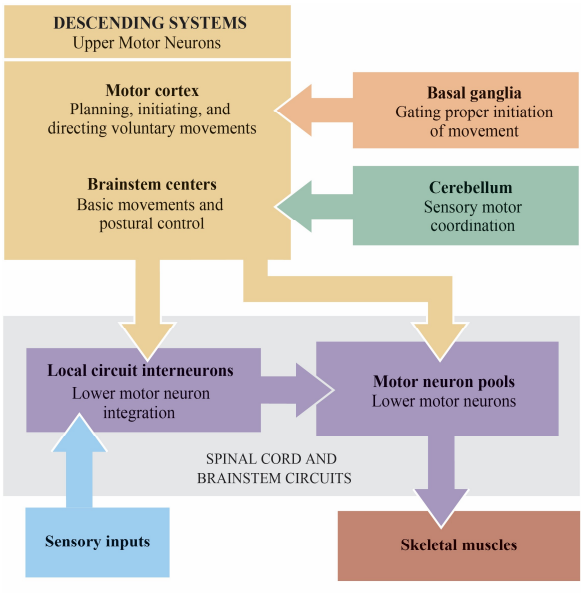

Figure 10 Schematic representation of the structures involved in motor control. The UMN receive information from the basal ganglia and cerebellum. The motor cortex integrates this information and projects to the spinal cord directly and indirectly through the brainstem and the local circuit interneurons. Figure adapted from [59].

brainstem centers, where sensory information is integrated into the local circuit interneurons and projected to the spinal cord, Figure 10 (adapted from [59]). Prioritizing reflexive over intrinsic modulation in the "up" strategy could be the result of faulty task-initiation. If hyperreflexia is present prior to initiation of the task, more sensory information is projected to the brainstem. Then, the task is initiated and performed in a state of overreliance on reflexive structures. Consequently, this mechanism is expected to underly the selection of the "up" strategy choice in patients with predominantly UMN degeneration.

The selection of the "down" strategy is expected to be related to two regions of the central nervous system. First, the reticular formation in the brain stem, which is involved in the organization of spatial and temporal movements [60]. Second, the basal ganglia are involved in initiation and performance of voluntary movements [61]. Both these systems have been shown to degenerate over time in ALS patients [62-64]. The loss of these UMN systems reduces the integration of sensorimotor information in the central command to the spinal cord. Then, more reliance on direct projections is required to perform motor tasks. Control based on direct projections is less accurate due to its feed-forward nature . When attempting to comply with a perturbation during the FTs, this inaccuracy would lead to marked increase in muscle stiffness k. Besides UMN degeneration, the choice of the "down" strategy could also originate from the loss of α-γ Motoneuron coactivation in the LMN [11]. Task performance under unpredictable conditions has been shown to require γ-motoneuron activity to increase muscle spindle sensitivity [59]. Such an alteration could also lead to more reliance on direct projections for control of the limb. As such, the origin of the "down" strategy cannot be fully explained by the results of this study. Though, the "up" strategy is most likely associated with the loss of UMN.

The FRFs during the PT of patients with reduced muscle strength contained a down-shifted resonance frequency compared to controls and their stronger peers. Therefore, an overlapping pathophysiological mechanism must exist between muscle strength and the resonance frequency. The modeled resonance frequency is primarily altered by the eigenfrequency of the muscle activation dynamics f_a and the neural delays τ. The death of large motor units in ALS leads to reinnervation of fast muscle fibers to slow muscle fibers [65]. The duration of the cross-bridge cycle in slow fibers is longer [66], effectively reducing the muscle activation dynamics f_a. Furthermore, conduction velocity of distal axons is reduced in ALS, which would lead to an increase in neural delays τ [67]. The eigenfrequencies of muscle activation dynamics f_a of ALS patients were indeed found to be lower than in controls (see Appendix F). However, the neural time delays τ of the patient group were comparable to the control group. Therefore, the shift of the resonance peak when performing PTs is most likely the result of altered muscle composition due to motor unit reinnervation. Examination of the intrinsic and reflexive parameters during the PT indicated that some participants relied predominantly on the augmentation of intrinsic parameters to resist the perturbations, i.e. co-contraction. Humans continuously adapt between energy efficient and costly strategies, such as reflexive and intrinsic control, to perform optimally with the least amount of energy [24]. In terms of task-performance, strong patients appeared to benefit more from energy-costly muscle co-contraction than their more atrophied counterparts. Some slightly weaker patients made the switch to more reflexive activity. Remarkably, the largest reflexive activity was found in the patients that swapped strategy during the FTs. However, the relation between strategy selection of the FTs and PT is not yet understood.

E. *Limitations*

1) Clinical measures and linear examination

Most qualitative measures for ALS are based on creating large position deviations of the limbs under passive conditions. In weak patients, the perturbation signal amplitude had to be reduced to maintain the wrist angle θ_{wrist} within a linear range. The reduced amplitude also diminished the velocity component of the signal [47]. As a result, inter-participant stimulation of muscle spindle velocity dependence k_v was altered. In continuation, activity from the muscle spindle position dependence k_p and the Golgi tendon organ force dependence k_f is more likely to be elicited under increased range of motion [55]. Yet, this study was able to capture overactive reflexes from proprioceptive afferents. Critical assessment into the derived reflexive parameters should be performed to exclude potential confounding factors.

2) Interpretation of active task results

The results from the active tasks were difficult to interpret due to the lack of comparable metrics for motor function. Suitable candidates for combination with this study would be electroencephalography (EEG) and electrodiagnostic threshold-tracking, as presented in the following studies [68-74]. Another limitation was the presence of noise in the measurements. Consequently, the validity of the parameter estimation procedure would likely improve by averaging the measurements over the trials, [46]. From a modeling perspective, the wrist was considered as a joint with a single bidirectional actuator. Yet in the FTs, some participants were suspected to only rely on co-contraction and release of the FCR to comply with the perturbations. To verify this statement, antagonistic (EMG-driven) models should be considered [32].

3) Small study group

An overarching limitation of the entire study, was the size of the study groups. A convenience sample of 10 ALS patients was recruited from separate studies that took place on the same day. The large diversity of the patient group, particularly in strength levels, makes interpretation of the study results difficult. Effective examination of the study parameters requires a larger, more clinically diverse and better stratified study population.

V. CONCLUSION

This study explored the feasibility of applying linear system identification (SI) and parameter estimation techniques on ALS, to quantify neuromuscular properties of patients under passive and active conditions. We have shown that ALS patients with large strength differences were able to participate in the study protocol. ALS patients were able to learn and perform the tasks similar to their healthy counterparts. Even though external validity was relatively low, the model was fitted with a high level of internal validity.

On a group level, the median muscle spindle position dependence k_p of ALS patients was significantly increased during the RT with respect to controls. The variance of the intrinsic properties from patients was found to be responsive to the variance of the MVC measurements. Examination of individual patients during the passive condition, i.e. the RT, showed that:

- Characteristic symptoms of UMN degeneration can be identified in the FRF in the presence of LMN degeneration;
- clinically recognized overactivity of reflexes in ALS originates from multiple reflexive pathways, not only the monosynaptic Ia stretch reflex;
- clinical scores of muscle tone, within two clinically recognized definitions, can be enhanced by the derived intrinsic parameters.

Examination of patients during the active task conditions, i.e. FTs and PT, showed that:

- the selection of control strategy for the FTs depends on the level of both UMN and LMN involvement;
- weaker patient rely much more on energy-efficient reflexive activity during the PTs than controls and stronger patients.

VI. RECOMMENDATIONS

The present study was of an exploratory nature. Consequently, several recommendations can be made for future work based on the acquired knowledge. Some of the recommendations relate to technical and analytical aspects, the remainder relates to the study design in general:

- We found evidence that the measurements were affected by time-variant behavior and visual feedback. Lowering the cutoff frequency of the visual feedback, could reduce the respective effects of these phenomena. Restricting the subject's attention more to the proprioception of the wrist might reduce spontaneous alterations in control strategy. To that extent, either the type of visual feedback could be altered, or task instructions could be altered enhance focus on the feeling in the wrist.
- The use of a virtual environment with damping and stiffness should be considered to increase the velocity component of the perturbation signal during the RT [52]. A similar approach could reduce the effect of the Wristalyzer's resonance peak on the FRFs during the FTs. Alternatively, the Wristalyzer could also be programmed to produce a bias torque with its motor. Introducing damping is recommended nonetheless [52].
- To improve the parameter estimation, we recommend analyzing the internal-external validity tradeoff to find the optimal value of weight q_i.
- Depending on the study goal, the use of a model with visual feedback should be considered. If absolute precision is required, a visual feedback model might improve the quantitative nature of this examination technique.
- An important focus of this study was the validity of the approach and the feasibility of the study protocol in a vulnerable patient group. Prior to continuing or adapting the study for future work, it is recommended to establish a large enough sample size within the presented framework. In addition, disease controls from purely LMN or UMN disorders should be considered, to validate whether UMN and LMN symptoms are accurately disentangled.

APPENDIX A PERTURBATION SIGNALS

During the Wristalyzer protocol, the limbs were perturbed with continuous multisine torque disturbances. The perturbation signals were designed to have rectangular power spectra with a bandwidth of 0.1 Hz - 0.7 Hz. To reduce the variance of the frequency response estimators, power was supplied at adjacent frequency points for averaging [49]. In addition, reduced power was added on frequencies up to 40 Hz according to the reduced-power method [44]. The frequency domain representation of the signal was transformed with inverse Fourier transformation to the time domain, yielding a 32s multisine signal with a sample frequency of 2048 Hz. The total time domain signal was elongated to yield a final 35s signal. This signal formed the basis for all the tests of the Wristalyzer protocol. The power of the torque between 0.1-0.7 Hz was scaled during the tasks according to

$$d_{ij}(t) = k_{ij} d_{fp}(t) + d_{rp}(t) \tag{8}$$

$$d_{ij}(t) = T_{bias}\left[k_{ij} d_{fp}(t) + d_{rp}(t)\right] \tag{9}$$

Where i denotes the task, j denotes the participant, d_{fp} the torque at dominant frequencies and d_{rp} the torque at frequencies with reduced power. The perturbation signal during RT and PT was scaled by Eq. 8. Bias torque during FTs was compensated by scaling the torque over its entire frequency range, Eq. 9. The torque amplitude k_{ij} of the dominant frequencies was determined during the training trials of the subjects. The full signal scaling factor T_{bias} for the force tasks was determined by the torque bias level. An example of the time- and frequency domain representation is depicted in Figure 11.

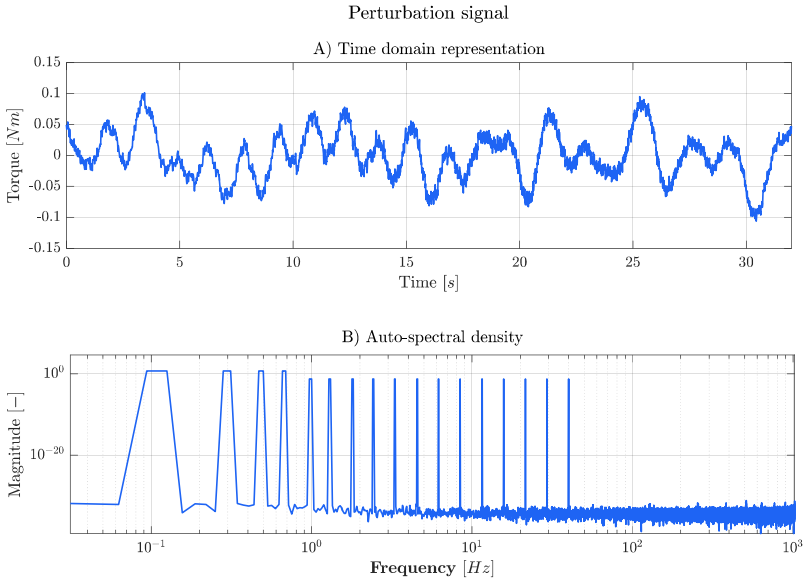

Figure 11 The default perturbation signal prior to alteration for the correction of inter-subject strength differences and inter-task differences in admittance. A) Presents the time-domain representation of the 32 s torque perturbation signal. B) Depicts the magnitude of the auto-spectral density of the perturbation signal in the frequency-domain.

APPENDIX B FLOWCHART OF DATA ANALYSIS

The neuromuscular parameters and model-predicted output signals are determined by following the flowchart in Figure 12. This procedure resembles the one described by [75]. Mechanical signals were cut to the appropriate length and detrended prior to resampling to remove drift and potential zero-offsets. Hereafter, the cross-spectral densities were estimated in order to derive the joint admittance. The EMG signals were detrended as well. After prewhitening, the EMG was summed to mimic a single continuous actuation signal of the wrist joint. Similar to the mechanical signals, the cross-spectral density was estimated after preprocessing for derivation of the reflexive impedance. The parameters derived from the parameter estimation were subsequently implemented in the model to simulate wrist torque and angle.

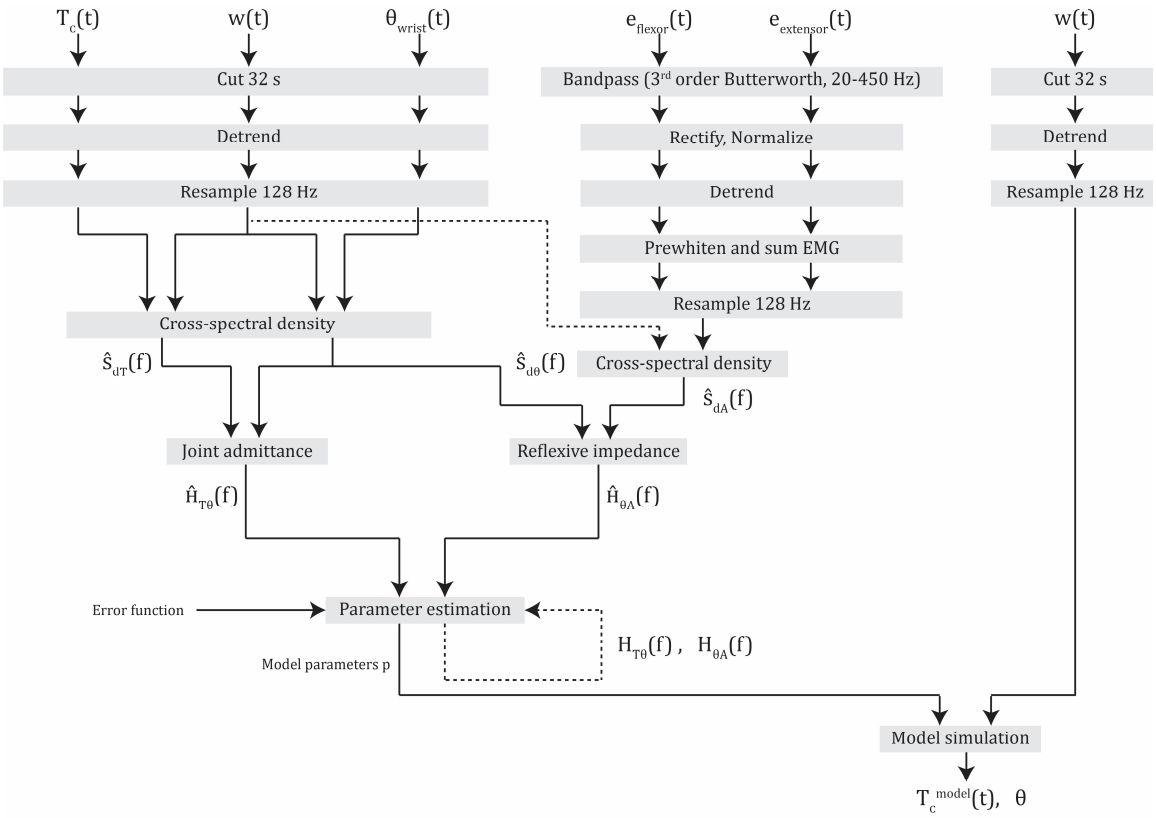

Figure 12 Flowchart of all the steps undertaken in this study. The derived joint admittance and reflexive impedance are the input to the error function, which is iteratively minimized. The minimization yields a set of neuromuscular parameters. The model is simulated with these parameters to generate the model-predicted torque and angle to the same perturbation signal *w(t)* for validation.

APPENDIX C NEUROMUSCULAR MODEL DERIVATION

The NMM that is used for deriving neuromuscular properties of the patients is based on a linearized Hill-type muscle model [76]. Although several studies have presented similar models [24, 28, 41, 43, 45], this appendix mainly serves as clarification of the equations describing the modeled joint admittance and reflexive impedance. For this purpose, it is imperative to discern between two main components. The first component characterizes the interaction of the human with the environment, i.e. the Wristalyzer. The second component describes the production of muscle force.

Interaction with the environment

In this particular study, participants are supplied with perturbations through the handle of the Wristalyzer. As a result, the effects of the Wristalyzer handle dynamics are taken into account. These handle dynamics can be described by a rotational second-order system, Eq. 10. Note that all the equations in this Appendix are given in frequency domain. Hence, variable *s* denotes the Laplace operator.

$$H_e = \frac{1}{I_{wl}s^2 + b_{wl}s + k_{wl,i}} \tag{10}$$

The respective variables I_{wl}, b_{wl} and k_{wl} denote the inertia, damping and stiffness of the Wristalyzer handle. The inertia of the Wristalyzer handle was determined to be 0.0022 kgm^2. The damping of the handle was kept at zero, as the motion of the handle is considered near frictionless. Bias torques during the FTs were achieved by introducing a non-zero rotational stiffness. The stiffness with respect to each task set to:

$$k_{wl} = [0, 0.1 \cdot MVC, 0.2 \cdot MVC, 0] \tag{11}$$

In addition, the effect of the grip strength on the transmission of torques from the Wristalyzer handle to the wrist joint are captured in the contact dynamics. These effects are described as a visco-elastic force, elicited by differences in the rotations of the handle $\theta_{wl}(t)$ and the wrist $\theta_{wrist}(t)$, Eq. 12.

$$H_c = b_c s + k_c \tag{12}$$

Muscle force production

The force production of the muscle is attributed to an intrinsic and a reflexive component. The intrinsic component is described as a visco-elastic element which relates the muscle stretch to muscle force, Eq.13. The values of intrinsic muscle stiffness, *k*, and viscosity, *b*, are elicited by the mean supraspinal command.

$$H_{ve} = bs + k \tag{13}$$

The reflexive component of the muscle force depends on the feedback from the proprioceptive organs, i.e. the muscle spindles and Golgi tendon organs. This reflexive activity is captured with EMG in the signal $A(s)$, Eq. 14.

$$A(s) = (H_{ms} - H_{ve}H_{gto}) \cdot H_{filtgto} \cdot \theta_{tot}(s) \tag{14}$$

The first contributors to $A(s)$ are the Golgi tendon organs, which are modeled as a scaling factor (i.e. gain) on the summed reflexive and intrinsic muscle force, Eq. 15. The second contributors to $A(s)$ are the muscle spindles, which are modeled as a position and velocity dependent resistance to muscle stretch, Eq. 16. However, it is important to note that muscle stretch is not directly related to the wrist rotation $\theta_{wrist}(s)$. The muscle is connected in series with a tendon, described as an element with finite stiffness k_{tend} , Eq. 17. The tendon stretch is subtracted from $\theta_{wrist}(s)$ to obtain the resulting muscle stretch $\theta_{tot}(s)$, Eq. 18. To account for the delays in the proprioceptive pathways and the lower motor neurons, a Padé filter is added to the transfer functions of the proprioceptive organs, Eqs. 15-16. In addition, due to the force feedback, the Golgi tendon organs effectively act as a filter on the muscle activation $A(s)$, Eq. 19.

$$H_{gto} = k_f e^{-\tau_{gto}s} \tag{15}$$

$$H_{ms} = (k_v s + k_p) \cdot e^{-\tau_{ms}s} \tag{16}$$

$$H_{tend} = k_{tend} \tag{17}$$

$$\theta_{tot}(s) = \theta_{wrist}(s) - H_{tend}T_{muscle}(s) \tag{18}$$

$$H_{filtgto} = \frac{1}{1+H_{act}H_{gto}} \tag{19}$$

Lastly, the reflexive contribution to muscle force is approximated by passing *A(s)* through a second order Butterworth filter, Eq. 20. The difference between the total torque produced by the muscle T_{muscle} and the contact torque T_c causes the rotation of $\theta_{wrist}(s)$ through inertia *I*, Eqs. 21-23.

$$H_{act} = \frac{1}{s^2+\frac{2b}{\omega_0}s+{\omega_0}^2} \tag{20}$$

$$T_{muscle}(s) = H_{act}A(s) + H_{ve}\theta_{tot}(s) \tag{21}$$

$$\theta_{wrist}(s) = (T_c(s) - T_{muscle}(s)) \cdot H_i \tag{22}$$

$$H_i = \frac{1}{Is^2} \tag{23}$$

Joint admittance and reflexive impedance

The modeled joint admittance is obtained by combining Eqs. 10, 19-23. The joint admittance of the human is derived through substitution of Eqs. 24-25 into Eq. 26. The admittance of the total system, thus including the Wristalyzer is presented in Eq. 27.

$$H_{fb} = H_{ve} + (H_{ms} - H_{ve}H_{gto}) \cdot H_{filtgto}H_{act} \tag{24}$$

$$H_{T\theta_{wrist}} = \frac{1}{H_i+H_{fb}\frac{H_{tend}}{H_{tend}+H_{fb}}} \tag{25}$$

$$H_{T\theta} = \frac{1}{H_c} + H_{T\theta_{wrist}} \tag{26}$$

$$H_{T\theta^*} = \frac{H_eH_{T\theta}}{H_{T\theta}+H_e} \tag{27}$$

The modeled reflexive impedance is obtained by combining Eqs. 14-20 into Eq. 28. With the introduction of contact dynamics, the final reflexive impedance is determined by Eq. 29.

$$H_{\theta_{wrist}A} = (H_{ms} - H_{ve}H_{gto}) \cdot H_{filtgto}\frac{H_{tend}}{H_{ten}+H_{fb}} \tag{28}$$

$$H_{\theta A} = H_{\theta_{wrist}A}\frac{H_cH_{T\theta_{wrist}}}{1+H_cH_{T\theta_{wrist}}} \tag{29}$$

APPENDIX D TIME DOMAIN MEASUREMENTS AND FREQUENCY RESPONSE FUNCTIONS

This appendix primarily serves as an illustration of the time-domain measurements, the spectral estimators and a typical model fit. During the RT and PT, wrist torque and wrist angle were expected to be in phase, whereas the wrist torque and EMG signal were expected to be in anti-phase [41]. Meaning that an increase in wrist torque was accompanied by an increase in wrist angle and an increase in the agonist's EMG. The opposite relation was expected in the FTs [41]. The described relation between the wrist torque T_c, wrist angle θ_{wrist} and flexor and extensor EMG e_{flexor} and $e_{extensor}$, was found throughout all RT and PT recordings, Figure 13A-D. However, the expected relation between the measurements of the $FT_{10\%}$ and $FT_{20\%}$ was not found in one patient and one control. Such an event can indicate that these participants were not able to perform the task, or simply did not understand it well enough. A typical perturbation signal and the resulting wrist torque T_c, wrist angle θ_{wrist} and flexor and extensor EMG e_{flexor} and $e_{extensor}$ are presented in Figure 13. The FRFs are presented on the next page.

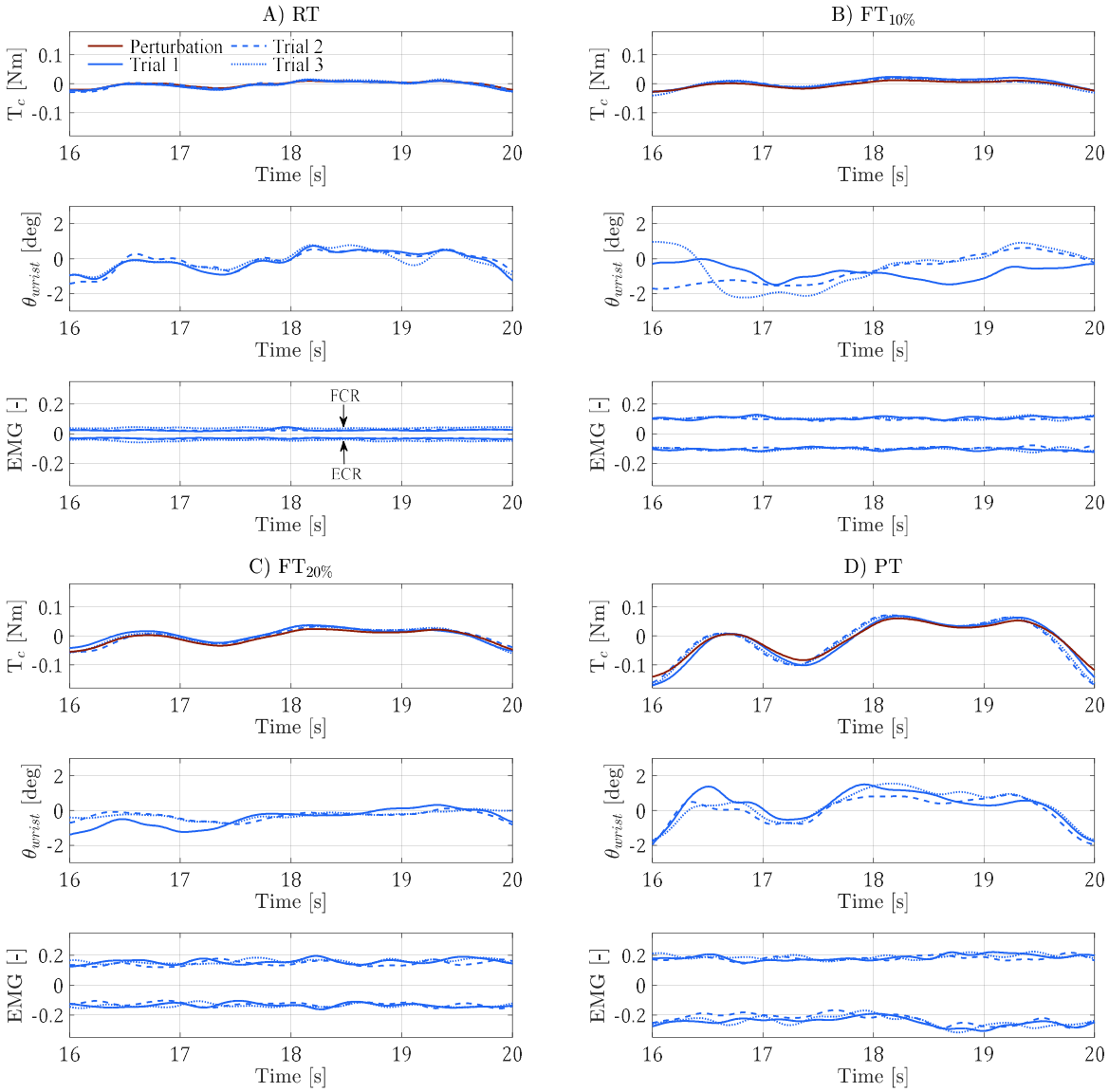

Figure 13 The measured wrist torque T_c, wrist angle θ_{wrist} and the flexor and extensor EMG e_{flexor} and $e_{extensor}$, of a typical ALS patient. The perturbation signal is depicted alongside the wrist torque T_c with the solid red line. Measurements of Trial 1, 2 and 3 are denoted by the blue solid, dashed and dotted lines respectively. A) Depicts the measurements of the RT, B) the $FT_{10\%}$, C) the $FT_{20\%}$ and D) the PT. The positive EMG signal has been derived from the FCR; the negative from the ECR. The measurements are shown within a 4s window and have been low-pass filtered (3rd order Butterworth) at 3 Hz for clarity.

The admittances during the RT and PT resembled a typical 2nd order system. The admittance of FTs presented similar behavior at frequencies upwards of 1Hz. However, at lower frequencies the FTs were characterized by a magnitude with a negative slope, indicative of compliant behavior. The phase at low frequencies was lowest during FTs (-90° to -45°), followed by the RT (-20° to 0°) and the PT (45° and 90°). Generally, the FRFs of each task were consistent over the three trials. An example illustrating the consistency and the general shape of the FRFs per task is presented in Figure 14.

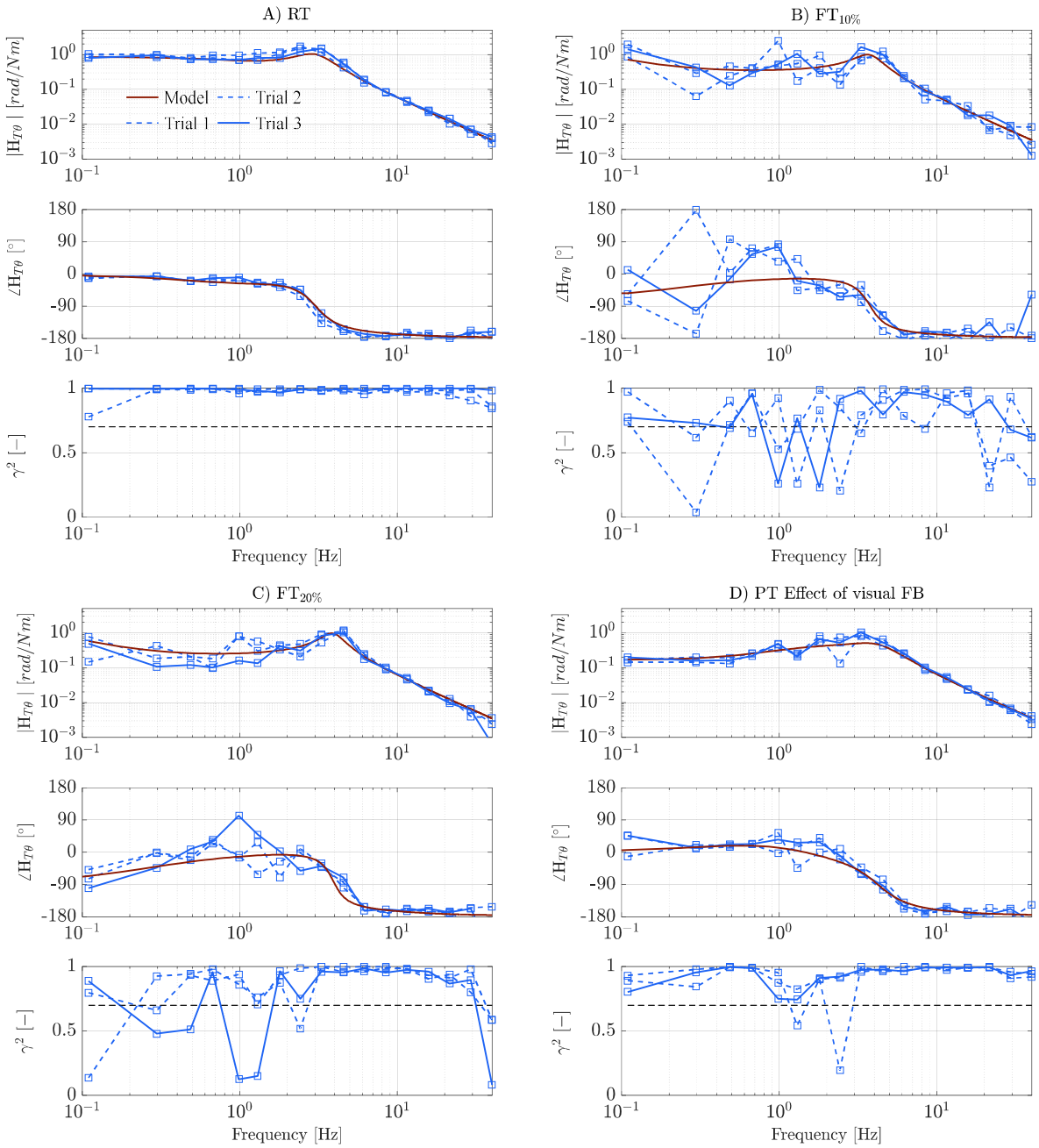

Figure 14 The FRF (magnitude $|\hat{\boldsymbol{H}}_{T\theta}|$ and phase $\angle\hat{\boldsymbol{H}}_{T\theta}$) and coherence $\boldsymbol{\gamma^2}$ of the joint admittance from an ALS patient. The model with the best VAFs was derived from the parameter set of trial 2, plotted as the red solid line. The FRFs and coherences from trial 1, 2 and 3 are depicted by the blue solid, dashed and dotted lines respectively. The FRFs and coherence are plotted exclusively on the frequencies excited by the perturbation signal, indicated by the square markers. The model FRF is plotted on all frequencies in the excited range of the perturbation signal. A) Depicts the measurements of the RT, B) the $FT_{10\%}$, C) the $FT_{20\%}$ and D) the PT.

APPENDIX E INTERNAL AND EXTERNAL MODEL VALIDITY

The sensitivity of the parameter estimation procedure in control and ALS group is expressed by the standard error of the mean (SEM), presented in Figure 15A-B. These depicted values are determined from all the trials per task per participant, i.e. each depicted value represents the mean and standard deviation of 3 x 9 (or 10) = 27 (or 30) SEMs. For legibility, the parameter names are given numerically. The task-dependent parameters are grouped as follows: 1-5, RT; 6-10, $FT_{10\%}$; 11-15 $FT_{20\%}$; 16-20, PT. The task-independent parameters are denoted by parameter numbers 21-28. Consequently, the order in which the task-dependent parameters are presented is: muscle viscosity b, muscle stiffness k, muscle spindle velocity dependence k_v, muscle spindle position dependence k_p and Golgi tendon organ force dependence k_f. The task-independent parameters are presented in the following order: joint inertia I, contact dynamics damping b_k, contact dynamics stiffness k_c, tendon stiffness k_{tend}, neural delay of the muscle spindles τ_{ms}, neural delay of the Golgi tendon organs, muscle activation filter eigenfrequency f_a and muscle activation filter damping β. With the exception of k_f in the RT of the ALS group, all SEM averages were below 2%.

Average group parameter interdependence, presented in the form of a heatmap, is depicted in Figure 15C-D. Most of the parameter interdependence values were extremely low. For legibility, the parameters have neither been numbered nor named. With the exception of the parameters enclosed by the square, the heatmap represents the interdependences of the task-dependent parameters in a similar manner as described above. In this case, trials have been taken separately and 60 task-dependent parameters are displayed. Consequently, columns 1-15 correspond to the RT, 16-30 to the $FT_{10\%}$, etc.. The values of these interdependences were very low, as can be visually inspected in Figure 15C-D. The enclosure contains the-task independent parameters, presented from left to right in the same order as mentioned earlier. The corresponding values were on average still below 6% in both groups. Note, the values on the diagonal have a value of 100%, though the limit of the heatmap has been set at 6% for visual inspection. Lastly, the best VAFs of the three trials per task and participant are presented in Table 4.

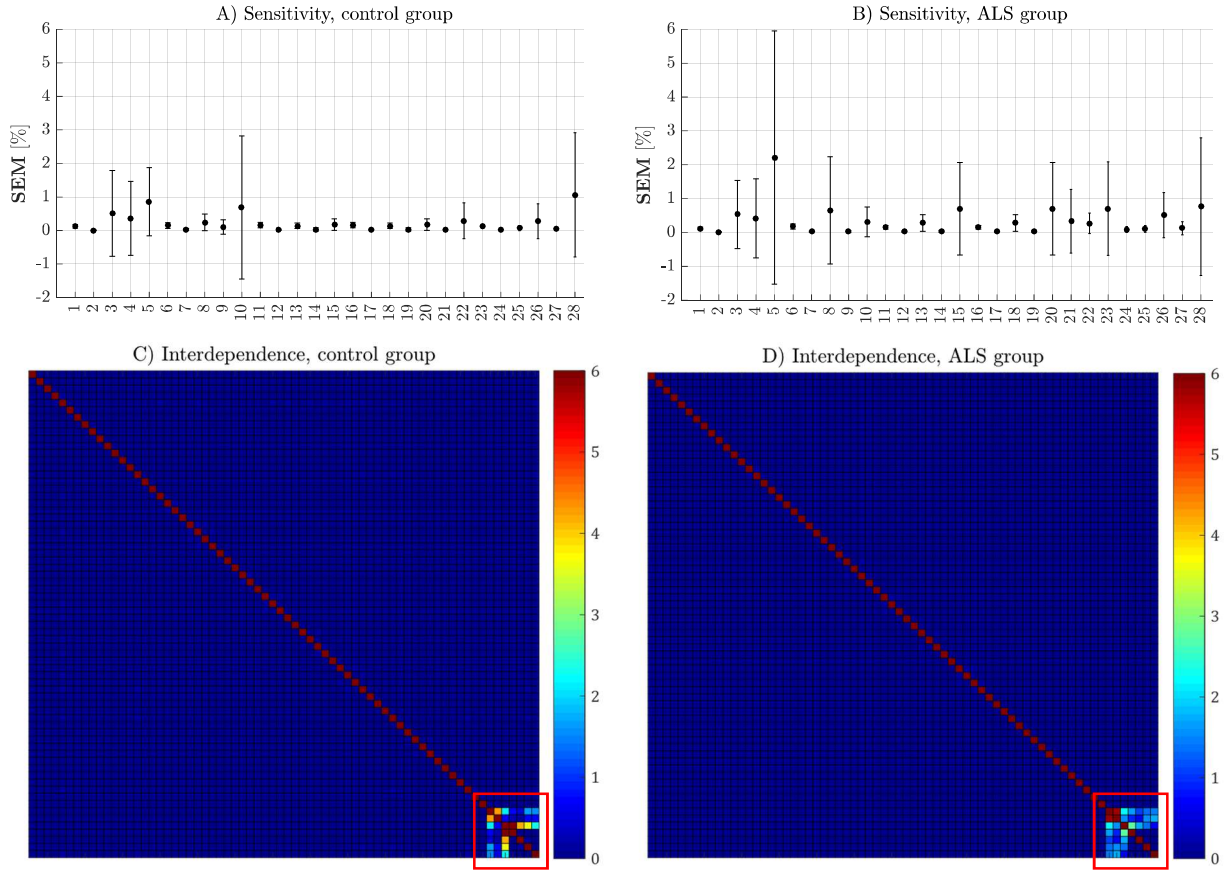

Figure 15 A) The sensitivity of the parameters of the control group expressed as standard error of the mean (SEM) values in percentages. B) The sensitivity of the parameters of the ALS group expressed as SEM in percentages. A-B) The markers denoted the group mean SEMs from one parameter, i.e. three per task per participant. The whiskers indicate the standard deviation. The numbering of the x-axis represents the corresponding parameter, as described in the text. C) The mean parameter interdependence of the control group expressed as percentages in a heatmap. D) The mean parameter interdependence of the ALS group, similarly expressed as C). C-D) Both heatmaps are symmetric, with the diagonal containing all auto-correlations of the parameters. The diagonal values are actually 100%, although displayed as 6% for visibility of smaller values. The red enclosures contain the values of the task-independent parameters. The order of presentation is given in the text.

Table 4 The best VAF from each of the three trials per task and participant. The VAF of the model-predicted wrist torque T_c was generally highest in the PT throughout all participants (VAF T_c > 84%). The highest VAFs of the wrist angle θ_{wrist} were consistently found in the RT. Three controls and one patient had negative VAFs in all trials of the PT.

		VAF T_c (%)				***VAF θ_{wrist} (%)***			
Group	Subject nr.	RT	$FT_{10\%}$	$FT_{20\%}$	PT	RT	$FT_{10\%}$	$FT_{20\%}$	PT
Controls	1	74,1	73,5	49,2	81,8	67,7	54,0	46,1	43,0
	2	92,8	57,8	68,4	95,6	89,5	48,6	51,9	-16,6
	3	95,3	88,7	82,2	95,8	89,1	33,3	23,9	-22,4
	4	90,7	94,4	87,8	96,2	87,1	69,8	22,5	-10,6
	5	92,2	83,6	87,4	96,3	86,9	35,2	51,4	35,0
	6	89,0	88,5	66,5	94,4	73,8	55,2	50,5	55,1
	7	89,8	88,6	88,1	94,6	91,3	70,0	33,7	68,0
	8	89,0	84,5	76,3	95,4	71,9	63,8	17,7	22,7
	9	95,0	73,4	41,4	93,8	87,4	36,7	63,8	25,4
ALS	1	74,0	73,3	72,2	83,9	74,6	44,1	27,4	56,2
	2	69,5	28,4	39,8	84,4	63,9	31,7	18,9	22,0
	3	94,0	81,5	70,9	96,2	87,1	50,4	52,5	24,0
	4	91,4	73,4	69,1	96,5	90,9	47,2	39,5	44,1
	5	79,5	70,4	80,0	96,3	78,5	13,3	52,8	32,1
	6	95,3	84,0	74,5	94,5	94,6	67,9	67,0	47,0
	7	70,3	76,6	85,0	96,2	65,5	11,9	34,9	67,4
	8	54,7	67,0	58,4	93,7	74,5	22,6	30,2	44,0
	9	75,8	78,0	73,8	95,1	72,5	66,6	37,9	56,5
	10	90,4	91,8	91,3	95,4	80,9	98,0	57,9	-65,7

APPENDIX F NEUROMECHANICAL PARAMETERS

A total of 68 parameters were derived from the neuromuscular model (NMM). Of these parameters, 60 were task-dependent and corrected with the MVC. The parameters yielding the highest VAF when simulating the model were selected per task. The group median and interquartile ranges of the remaining 28 parameters are presented in Table 5.

Table 5 Median and interquartile ranges of the model parameters in the control and patient groups. In addition to the task-dependent parameters, the task-independent parameters (TID) are presented in the bottom rows of this table.

		Controls	**Patients**	**Statistics**	
Task	Parameter	Median (IQR)	Median (IQR)	Median	Variance
RT	b	0.197 (0.144 - 0.239)	0.162 (0.126 - 0.198)	0.57	0.616
	k	2.94 (2.61 - 4.35)	1.97 (1.16 - 2.88)	0.0977	0.855
	k_v	0.0826 (0.0443 - 0.203)	0.153 (0.0793 - 0.203)	0.57	0.527
	k_p	0.0242 (-0.645 - 0.374)	0.819 (-0.0113 - 1.83)	0.0977	0.127
	k_f	-0.0545 (-0.232 - -0.00758)	-0.105 (-0.171 - 0.0525)	0.652	0.248
FT10	b	0.314 (0.221 - 0.39)	0.217 (0.201 - 0.339)	0.359	0.699
	k	4.75 (4.43 - 7.12)	3.56 (2.15 - 6.37)	0.57	0.788
	k_v	0.308 (0.193 - 0.388)	0.195 (0.156 - 0.329)	0.359	0.96
	k_p	-3.47 (-4.63 - 2.93)	-1.01 (-2.86 - 0.608)	1	0.0973
	k_f	-0.536 (-0.781 - -0.343)	-0.335 (-0.622 - -0.161)	0.203	0.454
FT20	b	0.333 (0.262 - 0.509)	0.369 (0.162 - 0.467)	0.359	0.841
	k	5.9 (4.34 - 7.09)	4.48 (2.1 - 7.18)	0.734	0.259
	k_v	0.185 (-0.0641 - 0.433)	0.138 (-0.0113 - 0.445)	0.82	0.506
	k_p	-1.02 (-5.04 - 3.37)	-2.04 (-6.28 - -0.519)	0.57	0.93
	k_f	-0.61 (-0.746 - -0.23)	-0.466 (-0.785 - -0.373)	0.91	0.39
PT	b	0.272 (0.17 - 0.316)	0.173 (0.139 - 0.224)	0.195	0.214
	k	5.87 (5.27 - 7.29)	5.81 (4.13 - 6.85)	0.313	0.644
	k_v	-0.00817 (-0.126 - 0.0985)	0.0204 (-0.146 - 0.0872)	0.844	0.392
	k_p	-0.628 (-1.8 - 1.94)	0.576 (-0.765 - 2.36)	0.945	0.705
	k_f	-0.699 (-0.825 - -0.452)	-0.592 (-0.768 - -0.0959)	0.945	0.367
TID	I	0.00435 (0.00426 - 0.00508)	0.00485 (0.00445 - 0.00557)	-	-
	b_c	174 (121 - 335)	160 (119 - 227)	-	-
	k_c	451 (366 - 839)	405 (286 - 656)	-	-
	k_{tend}	1.31e+03 (1.05e+03 - 1.88e+03)	1.33e+03 (1.09e+03 - 1.53e+03)	-	-
	τ_{ms}	0.0342 (0.0322 - 0.0359)	0.0315 (0.03 - 0.0353)	-	-
	τ_{gto}	0.0251 (0.0203 - 0.0284)	0.0215 (0.0187 - 0.0305)	-	-
	f_a	7.69 (6.64 - 8.33)	6.4 (4.2 - 7.8)	-	-
	β	0.966 (0.898 - 1.09)	1.06 (0.897 - 1.23)	-	-

APPENDIX G MODELING VISUAL FEEDBACK

With the use of NMClab [45], the effect of neural delays of the Golgi tendon organs and muscle spindles on the FRFs was examined, Figures 16A-B. Increasing neural delays can alter the physiological significance of the feedback mechanism. Hence, the nomenclature force and position feedback is preferred. Increasing the delay of the position feedback upwards of 150ms and higher introduced the behavior identified from the FRF. However, this latency is decidedly longer than even the long-latency (M2) reflex (~50-100ms) [77]. Visual feedback also has a very long latency, although it is only an effective mechanism for postural control up to ~0.5-1.0 Hz [78, 79]. To assess the contribution of visual feedback on the FRF of the wrist, a separate feedback pathway was added to the NMM [75]. The model-fit from one participant is presented in the discussion.

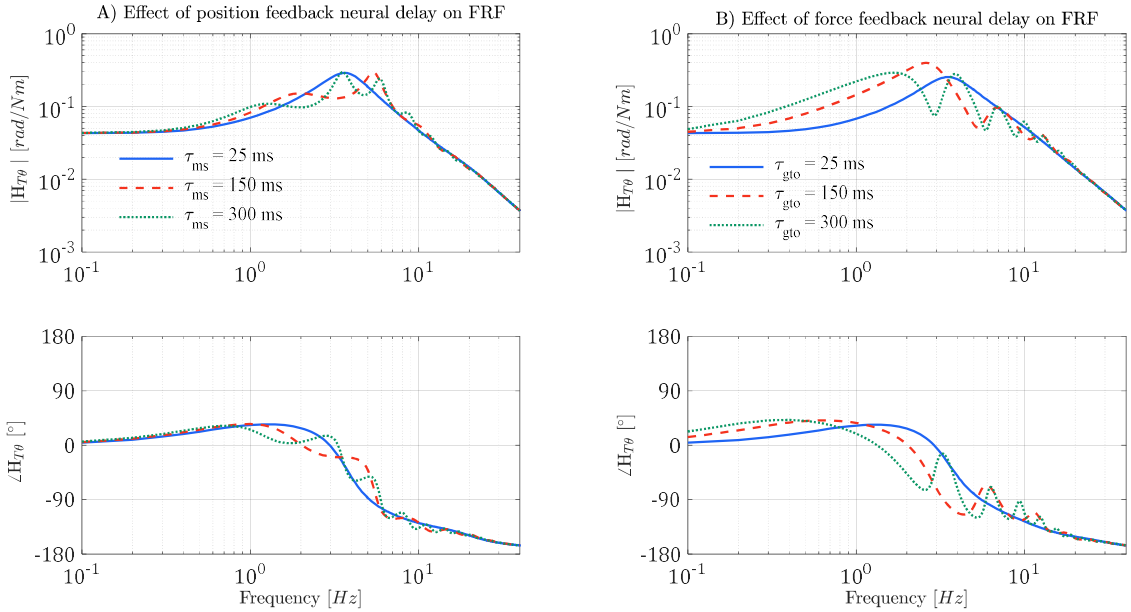

Figure 16 A) The effect of altering the position feedback by means of the muscle spindle delay of the model from 25ms, to 150ms and 300ms (solid, dashed and dotted blue lines, respectively). B) The effect of altering the force feedback by means of the Golgi tendon organ neural delay of the model from 25ms, to 150ms and 300ms (solid, dashed and dotted blue lines, respectively).

The new pathway takes into account the total computational delay, the filtering of the raw signal for displaying purposes and the humans response to the visual information. The computational delay was modeled as a Padé approximation:

$$H_{comp} = e^{(-s\tau_c)} \tag{30}$$

With τ_c the processing time, which is 62.5 ms. Prior to displaying, the visual information was low-pass filtered with a 2nd order Butterworth filter at 1 Hz:

$$H_{vfilt} = \frac{1}{s^2+\frac{2b}{\omega_0}s+{\omega_0}^2} \tag{31}$$

With b=1.41 and $\omega_0 = 6\pi$. The response of the wrist to the visual information was approximated as a velocity-dependent gain with a large time delay:

$$H_{vis} = k_{vis}se^{(-s\tau_{vis})} \tag{32}$$

The parameters k_{vis} and τ_{vis} were added to the parameter vector for optimization. As such, the parameter vector was supplied with 12 instances of k_{vis} and 1 instance of τ_{vis}. The bounds and initial values are presented in Table 6.

Parameter	Physiogical representation	Initial value	LB	UB	Unit
k_{vis}	Velocity dependent feedback gain	1	-10	10	Nms/rad
τ_{vis}	Neural delay of visual feedback	250	100	500	ms

Table 6 Additional parameters for the model with visual feedback, including the initial values, lower and upper bounds (LB and UB, respectively).

BIBLIOGRAPHY

[1] T. Lenglet, and J. P. Camdessanche, "Amyotrophic lateral sclerosis or not: Keys for the diagnosis," *Revue Neurologique,* vol. 173, no. 5, pp. 280-287, May, 2017.

[2] M. A. van Es, O. Hardiman, A. Chio, A. Al-Chalabi, R. J. Pasterkamp, J. H. Veldink, and L. H. van den Berg, "Amyotrophic lateral sclerosis," *Lancet (London, England),* vol. 390, no. 10107, pp. 2084-2098, 2017.

[3] M. C. Kiernan, S. Vucic, B. C. Cheah, M. R. Turner, A. Eisen, O. Hardiman, J. R. Burrell, and M. C. Zoing, "Amyotrophic lateral sclerosis," *The Lancet,* vol. 377, no. 9769, pp. 942-955, 2011.

[4] M. Swash, and R. Hutchison, *Hutchison's clinical methods*: Saunders, 2002.

[5] M. Swash, "Why are upper motor neuron signs difficult to elicit in amyotrophic lateral sclerosis?," *Journal of neurology, neurosurgery, and psychiatry,* vol. 83, no. 6, pp. 659-62, 2012.

[6] V. Dietz, and T. Sinkjaer, "Spastic movement disorder: impaired reflex function and altered muscle mechanics," *Lancet Neurology,* vol. 6, no. 8, pp. 725-733, Aug, 2007.

[7] A. Klomp, J. Van der Krogt, C. Meskers, J. De Groot, and E. De Vlugt, "Design of a concise and comprehensive protocol for post stroke neuromechanical assessment," *Bioeng Biomed Sci. S,* vol. 1, 2012.

[8] C. G. M. Meskers, J. H. de Groot, E. de Vlugt, and A. C. Schouten, "NeuroControl of movement: system identification approach for clinical benefit," *Frontiers in Integrative Neuroscience,* vol. 9, Sep 8, 2015.

[9] J. Valls-Sole, R. Alvarez, and E. S. Tolosa, "Vibration-induced presynaptic inhibition of the soleus H reflex is temporarily reduced by cortical magnetic stimulation in human subjects," *Neuroscience letters,* vol. 170, no. 1, pp. 149-152, 1994.

[10] J. W. Lance, "Pathophysiology of spasticity and clinical experience with baclofen," *Spasticity: disordered motor control*, pp. 185-204, 1980.

[11] M. Swash, and K. P. Fox, "The pathology of the human muscle spindle: effect of denervation," *J Neurol Sci,* vol. 22, no. 1, pp. 1-24, May, 1974.

[12] B. Stephens, R. J. Guiloff, R. Navarrete, P. Newman, N. Nikhar, and P. Lewis, "Widespread loss of neuronal populations in the spinal ventral horn in sporadic motor neuron disease. A morphometric study," *J Neurol Sci,* vol. 244, no. 1-2, pp. 41-58, May 15, 2006.

[13] W. Vattanasilp, L. Ada, and J. Crosbie, "Contribution of thixotropy, spasticity, and contracture to ankle stiffness after stroke," *Journal of Neurology, Neurosurgery & Psychiatry,* vol. 69, no. 1, pp. 34-39, 2000.

[14] A. L. Hof, "Changes in muscles and tendons due to neural motor disorders: implications for therapeutic intervention," *Neural plasticity,* vol. 8, no. 1-2, pp. 71-81, 2001.

[15] R. L. Lieber, S. Steinman, I. A. Barash, and H. Chambers, "Structural and functional changes in spastic skeletal muscle," *Muscle & nerve,* vol. 29, no. 5, pp. 615-27, 2004.

[16] J.-M. Gracies, "Pathophysiology of spastic paresis. I: Paresis and soft tissue changes," *Muscle & nerve,* vol. 31, no. 5, pp. 535-51, 2005.

[17] J.-M. Gracies, "Pathophysiology of spastic paresis. II: Emergence of muscle overactivity," *Muscle & nerve,* vol. 31, no. 5, pp. 552-71, 2005.

[18] M. M. Mirbagheri, C. Tsao, and W. Z. Rymer, "Natural history of neuromuscular properties after stroke: a longitudinal study," *Journal of neurology, neurosurgery, and psychiatry,* vol. 80, no. 11, pp. 1212-7, 2009.

[19] L. R. Smith, K. S. Lee, S. R. Ward, H. G. Chambers, and R. L. Lieber, "Hamstring contractures in children with spastic cerebral palsy result from a stiffer extracellular matrix and increased in vivo sarcomere length," *The Journal of physiology,* vol. 589, no. Pt 10, pp. 2625-39, 2011.

[20] H. van der Kooij, and F. C. T. van der Helm, "Observations from unperturbed closed loop systems cannot indicate causality," *Journal of Physiology-London,* vol. 569, no. 2, pp. 705-705, Dec 1, 2005.

[21] S. F. Campfens, A. C. Schouten, M. J. A. M. van Putten, and H. van der Kooij, "Quantifying connectivity via efferent and afferent pathways in motor control using coherence measures and joint position perturbations," *Experimental Brain Research,* vol. 228, no. 2, pp. 141-153, Jul, 2013.

[22] D. T. Westwick, and E. J. Perreault, "Closed-loop identification: application to the estimation of limb impedance in a compliant environment," *IEEE Transactions on Biomedical Engineering,* vol. 58, no. 3, pp. 521-530, 2010.

[23] R. J. Peterka, "Sensorimotor integration in human postural control," *Journal of Neurophysiology,* vol. 88, no. 3, pp. 1097-1118, Sep, 2002.

[24] F. C. T. van der Helm, A. C. Schouten, E. de Vlugt, and G. G. Brouwn, "Identification of intrinsic and reflexive components of human arm dynamics during postural control," *Journal of Neuroscience Methods,* vol. 119, no. 1, pp. 1-14, Sep 15, 2002.

[25] J. J. Palazzolo, M. Ferraro, H. I. Krebs, D. Lynch, B. T. Volpe, and N. Hogan, "Stochastic estimation of arm mechanical impedance during robotic stroke rehabilitation," *Ieee Transactions on Neural Systems and Rehabilitation Engineering,* vol. 15, no. 1, pp. 94-103, Mar, 2007.

[26] B. T. Volpe, P. T. Huerta, J. L. Zipse, A. Rykman, D. Edwards, L. Dipietro, N. Hogan, and H. I. Krebs, "Robotic Devices as Therapeutic and Diagnostic Tools for Stroke Recovery," *Archives of Neurology,* vol. 66, no. 9, pp. 1086-1090, Sep, 2009.

[27] E. de Vlugt, A. C. Schouten, and F. C. van der Helm, "Closed-loop multivariable system identification for the characterization of the dynamic arm compliance using continuous force disturbances: a model study," *Journal of neuroscience methods,* vol. 122, no. 2, pp. 123-140, 2003.

[28] A. C. Schouten, E. Vlugt, and F. C. T. van der Helm, "Design of perturbation signals for the estimation of proprioceptive reflexes," *Ieee Transactions on Biomedical Engineering,* vol. 55, no. 5, pp. 1612-1619, May, 2008.

[29] H. J. M. van der Krogt, C. G. M. Meskers, J. H. de Groot, A. Klomp, and J. H. Arendzen, "The gap between clinical gaze and systematic assessment of movement disorders after stroke," *Journal of Neuroengineering and Rehabilitation,* vol. 9, Aug 27, 2012.

[30] E. de Vlugt, J. H. de Groot, K. E. Schenkeveld, J. H. Arendzen, F. C. T. van der Helm, and C. G. M. Meskers, "The relation between neuromechanical parameters and Ashworth score in stroke patients," *Journal of Neuroengineering and Rehabilitation,* vol. 7, Jul 27, 2010.

[31] K. L. de Gooijer-van de Groep, E. de Vlugt, J. H. de Groot, H. C. M. van der Heijden-Maessen, D. H. M. Wielheesen, R. S. van Wijlen-Hempel, J. H. Arendzen, and C. G. M. Meskers, "Differentiation between non-neural and neural contributors to ankle joint stiffness in cerebral palsy," *Journal of Neuroengineering and Rehabilitation,* vol. 10, Jul 23, 2013.

[32] K. L. de Gooijer-van de Groep, E. de Vlugt, H. J. van der Krogt, A. Helgadottir, J. H. Arendzen, C. G. M. Meskers, and J. H. de Groot, "Estimation of tissue stiffness, reflex activity, optimal muscle length and slack length in stroke patients using an electromyography driven antagonistic wrist model," *Clinical Biomechanics,* vol. 35, pp. 93-101, Jun, 2016.

[33] H. van der Krogt, A. Klomp, J. H. de Groot, E. de Vlugt, F. C. T. van der Helm, C. G. M. Meskers, and J. H. Arendzen, "Comprehensive neuromechanical assessment in stroke patients: reliability and responsiveness of a protocol to measure neural and non-neural wrist properties," *Journal of Neuroengineering and Rehabilitation,* vol. 12, Mar 13, 2015.

[34] H. Zetterberg, G. E. Frykberg, J. Gaverth, and P. G. Lindberg, "Neural and Nonneural Contributions to Wrist Rigidity in Parkinson's Disease: An Explorative Study Using the NeuroFlexor," *Biomed Research International*, 2015.

[35] R. P. Xia, A. Muthumani, Z. H. Mao, and D. W. Powell, "Quantification of neural reflex and muscular intrinsic contributions to parkinsonian rigidity," *Experimental Brain Research,* vol. 234, no. 12, pp. 3587-3595, Dec, 2016.

[36] B. R. Brooks, R. G. Miller, M. Swash, and T. L. Munsat, "El Escorial revisited: revised criteria for the diagnosis of amyotrophic lateral sclerosis," *Amyotrophic lateral sclerosis and other motor neuron disorders,* vol. 1, no. 5, pp. 293-299, 2000.

[37] J. De Groot, D. Jägers, C. Meskers, A. Schouten, E. De Vlugt, and J. Arendzen, "Instrumented stretch reflexes of flexor carpi radialis and flexor carpi ulnaris muscle."

[38] E. F. Hodson-Tole, I. D. Loram, and T. M. M. Vieira, "Myoelectric activity along human gastrocnemius medialis: Different spatial distributions of postural and electrically elicited surface potentials," *Journal of Electromyography and Kinesiology,* vol. 23, no. 1, pp. 43-50, Feb, 2013.

[39] G. Grimaldi, P. Lammertse, N. Van Den Braber, J. Meuleman, and M. Manto, "A new myohaptic device to assess wrist function in the lab and in the clinic–the wristalyzer." pp. 33-42.

[40] E. A. Clancy, E. L. Morin, and R. Merletti, "Sampling, noise-reduction and amplitude estimation issues in surface electromyography," *Journal of Electromyography and Kinesiology,* vol. 12, no. 1, pp. 1-16, Feb, 2002.

[41] W. Mugge, D. A. Abbink, A. C. Schouten, J. P. A. Dewald, and F. C. T. van der Helm, "A rigorous model of reflex function indicates that position and force feedback are flexibly tuned to position and force tasks," *Experimental Brain Research,* vol. 200, no. 3-4, pp. 325-340, Jan, 2010.

[42] R. E. Kearney, R. B. Stein, and L. Parameswaran, "Identification of intrinsic and reflex contributions to human ankle stiffness dynamics," *Ieee Transactions on Biomedical Engineering,* vol. 44, no. 6, pp. 493-504, Jun, 1997.

[43] E. de Vlugt, A. C. Schouten, and F. C. T. van der Helm, "Quantification of intrinsic and reflexive properties during multijoint arm posture," *Journal of Neuroscience Methods,* vol. 155, no. 2, pp. 328-349, Sep 15, 2006.

[44] W. Mugge, D. A. Abbink, and F. C. T. van der Helm, "Reduced Power Method: how to evoke low-bandwidth behaviour while estimating full-bandwidth dynamics," *2007 Ieee 10th International Conference on Rehabilitation Robotics, Vols 1 and 2*, pp. 575-581, 2007.
[45] A. C. Schouten, W. Mugge, and F. C. T. van der Helm, "NMC1ab, a model to assess the contributions of muscle visco-elasticity and afferent feedback to joint dynamics," *Journal of Biomechanics,* vol. 41, no. 8, pp. 1659-1667, 2008.
[46] A. C. Schouten, E. De Vlugt, J. J. B. Van Hilten, and F. C. T. Van der Helm, "Quantifying proprioceptive reflexes during position control of the human arm," *Ieee Transactions on Biomedical Engineering,* vol. 55, no. 1, pp. 311-321, Jan, 2008.
[47] C. G. M. Meskers, A. C. Schouten, J. H. de Groot, E. de Vlugt, B. J. J. van Hilten, F. C. T. Van der Helm, and H. J. H. Arendzen, "Muscle weakness and lack of reflex gain adaptation predominate during post-stroke posture control of the wrist," *Journal of Neuroengineering and Rehabilitation,* vol. 6, Jul 23, 2009.
[48] P. Welch, "The use of fast Fourier transform for the estimation of power spectra: a method based on time averaging over short, modified periodograms," *IEEE Transactions on audio electroacoustics,* vol. 15, no. 2, pp. 70-73, 1967.
[49] R. Pintelon, and J. Schoukens, *System identification: a frequency domain approach*: John Wiley & Sons, 2012.
[50] J. Schoukens, and R. Pintelon, "Measurement of frequency response functions in noisy environments," *IEEE Transactions on Instrumentation and Measurement,* vol. 39, no. 6, pp. 905-909, 1990.
[51] L. Ljung, "Issues in system identification," *IEEE Control Systems Magazine,* vol. 11, no. 1, pp. 25-29, 1991.
[52] M. P. Vlaar, and A. C. Schouten, "System identification for human motion control." pp. 600-605.
[53] E. Pierrot-Deseilligny, and D. Burke, *The circuitry of the human spinal cord: its role in motor control and movement disorders*: Cambridge University Press, 2005.
[54] E. M. Raynor, and J. M. Shefner, "Recurrent inhibition is decreased in patients with amyotrophic lateral sclerosis," *Neurology,* vol. 44, no. 11, pp. 2148-2148, 1994.
[55] V. Dietz, "Proprioception and locomotor disorders," *Nature Reviews Neuroscience,* vol. 3, no. 10, pp. 781, 2002.
[56] M. L. Latash, and V. M. Zatsiorsky, "5 - Muscle Tone," *Biomechanics and Motor Control*, M. L. Latash and V. M. Zatsiorsky, eds., pp. 85-98, San Diego: Academic Press, 2016.
[57] C. S. Sherrington, R. Creed, D. Denny-Brown, J. C. Eccles, E. Liddell, R. S. Creed, and D. D. E. Denny-Brown, *Reflex activity of the spinal cord*: Oxford University Press (printed by Lowe and Brydone), 1932.
[58] H. G. J. M. Kuypers, and G. F. Martin, *Descending pathways to the spinal cord*: Elsevier, 2011.
[59] D. Purves, G. Augustine, D. Fitzpatrick, L. Katz, A. LaMantia, J. McNamara, and S. J. N. n. e. S. Williams, MA: Sinauer Associates, "Chapter 17: Upper motor neuron control of the brainstem and spinal chord," 2001.
[60] B. Sjolund, and A. Bjorklund, "Brain Stem Control of Spinal Mechanisms," Amsterdam: Elsevier, 1982.
[61] H. J. Groenewegen, "The basal ganglia and motor control," *Neural plasticity,* vol. 10, no. 1-2, pp. 107-120, 2003.
[62] M. C. Smith, "Nerve fiber degeneration in the brain in amyotrophic lateral sclerosis," *Journal of neurology, neurosurgery, and psychiatry,* vol. 23, no. 4, pp. 269-282, 1960.
[63] P. Bede, M. Elamin, S. Byrne, R. L. McLaughlin, K. Kenna, A. Vajda, N. Pender, D. G. Bradley, and O. Hardiman, "Basal ganglia involvement in amyotrophic lateral sclerosis," vol. 81, no. 24, pp. 2107-2115, 2013.
[64] J. T. Hughes, Advances in neurology, "Pathology of amyotrophic lateral sclerosis," vol. 36, pp. 61-74, 1982.
[65] A. Abraham, and V. E. Drory, "Fatigue in motor neuron diseases," *Neuromuscular Disorders,* vol. 22, pp. S198-S202, 2012/12/01/, 2012.
[66] J. M. Metzger, and R. L. Moss, "Calcium-sensitive cross-bridge transitions in mammalian fast and slow skeletal muscle fibers," vol. 247, no. 4946, pp. 1088-1090, 1990.
[67] K. R. Sharma, and R. G. Miller, "Electrical and mechanical properties of skeletal muscle underlying increased fatigue in patients with amyotrophic lateral sclerosis," *Muscle & Nerve,* vol. 19, no. 11, pp. 1391-1400, 1996.
[68] M. P. Vlaar, T. Solis-Escalante, A. N. Vardy, F. C. Van Der Helm, and A. C. Schouten, "Quantifying nonlinear contributions to cortical responses evoked by continuous wrist manipulation," *IEEE transactions on neural systems rehabilitation engineering,* vol. 25, no. 5, pp. 481-491, 2016.
[69] M. Vlaar, "Characterizing Cortical Responses Evoked by Robotic Joint Manipulation after Stroke," Delft University of Technology, 2017.
[70] M. P. Vlaar, T. Solis-Escalante, J. P. Dewald, E. E. Van Wegen, A. C. Schouten, G. Kwakkel, and F. C. Van Der Helm, "Quantification of task-dependent cortical activation evoked by robotic continuous wrist

joint manipulation in chronic hemiparetic stroke," *Journal of neuroengineering rehabilitation,* vol. 14, no. 1, pp. 30, 2017.
[71] S. F. Campfens, S. B. Zandvliet, C. G. M. Meskers, A. C. Schouten, M. J. A. M. van Putten, and H. van der Kooij, "Poor motor function is associated with reduced sensory processing after stroke," *Experimental Brain Research,* vol. 233, no. 4, pp. 1339-1349, April 01, 2015.
[72] S. F. Campfens, C. G. M. Meskers, A. C. Schouten, M. J. A. M. v. Putten, and H. v. d. Kooij, "Stretch Evoked Potentials in Healthy Subjects and After Stroke: A Potential Measure for Proprioceptive Sensorimotor Function," *IEEE Transactions on Neural Systems and Rehabilitation Engineering,* vol. 23, no. 4, pp. 643-654, 2015.
[73] S. Zandvliet, E. van Wegen, S. Campfens, H. van der Kooij, G. Kwakkel, and C. G. M. Meskers, "Position-cortical coherence as a marker for somatosensory integrity early post-stroke, a prospective cohort study."
[74] B. Sleutjes, I. Montfoort, E. Maathuis, J. Drenthen, P. van Doorn, G. H. Visser, and J. J. C. N. Blok, "CMAP scan discontinuities: automated detection and relation to motor unit loss," vol. 125, no. 2, pp. 388-395, 2014.
[75] D. A. Abbink, "Neuromuscular analysis of haptic gas pedal feedback during car following," 2006.
[76] A. V. Hill, "The heat of shortening and the dynamic constants of muscle," *Proc. R. Soc. Lond. B,* vol. 126, no. 843, pp. 136-195, 1938.
[77] J. A. Pruszynski, I. Kurtzer, and S. H. Scott, "The long-latency reflex is composed of at least two functionally independent processes," *Journal of neurophysiology,* vol. 106, no. 1, pp. 449-459, 2011.
[78] J. Dichgans, and T. Brandt, "Visual-vestibular interaction: Effects on self-motion perception and postural control," *Perception*, pp. 755-804: Springer, 1978.
[79] H. C. Diener, J. Dichgans, W. Bruzek, and H. Selinka, "Stabilization of human posture during induced oscillations of the body," *Experimental Brain Research,* vol. 45, no. 1, pp. 126-132, January 01, 1982.